Outage Performance of Relay-Assisted Mutualistic Backscatter Communications Under Energy-Causality Constraint

Yinghui Ye, Yujia Tian, Xiaoli Chu, *Senior Member, IEEE*, Sumei Sun, *Fellow, IEEE*, and Guangyue Lu

***Abstract*—Existing works on mutualistic backscatter communications (MBC) rely on the existence of direct links connecting both the primary user (PU) and the backscatter device (BD) to the destination node (D), rendering them ineffective when these links are blocked. While relay technology offers a solution, the performance of relay-assisted MBC and whether the backscatter link still benefits the primary link or not remain unclear. Additionally, the energy-harvesting capability of BD has been largely ignored in the study of MBC. This paper investigates a relay-assisted MBC network, where a decode-and-forward relay (R) forwards the messages of a PU and an energy constrained BD to D. We propose three forwarding schemes for R, i.e., orthogonal time-division multiple access (OMA), non-orthogonal multiple access (NOMA) with static power allocation (PA), and NOMA with dynamic PA. Considering the energy-causality constraint of BD, we derive the outage probabilities and diversity gains of the primary and backscatter links for each forwarding scheme. Computer simulation verifies the correctness of our analytical results and reveals that different from conventional MBC, in the relay-assisted MBC, whether or not the backscatter link improves the primary link's outage performance depends on the specific forwarding scheme employed, as well as the location of R and the power reflection coefficient of BD.**

***Index Terms*—Mutualistic backscatter communication, relay, outage performance.**

I. Introduction

The 3rd Generation Partnership Project (3GPP) has initiated studies on ambient Internet-of-Things (A-IoT), characterized by massive ultra-low complexity and ultra-low power devices [1]. The massive A-IoT devices are anticipated to be battery-less or equipped with limited energy storage, and thus may rely on passive communication technologies such as cooperative backscatter communication (BC) [2]–[5]. In cooperative BC, a backscatter device (BD), which can be an A-IoT device, modulates and reflects the incident signal from a primary user (PU) to its associated destination (D) [5]–[8], and D performs successive interference cancellation (SIC) to recover the information sent by the BD and the PU. Depending on whether the BD's symbol duration is much longer than that of the PU or not, cooperative BC can be classified into parasitic BC (PBC) and mutualistic BC (MBC) [6], [7]. In PBC, the symbol durations of the BD and the PU are comparable, thus the BD's reflected signal introduces co-channel interference to the primary link [7]. In MBC, as the symbol duration of the BD is much longer than that of the PU, the signal reflected by the BD can be regarded as an additional multi-path component of the PU's signal and may enhance the transmission performance of the PU [7].

1) Related Works on PBC: The authors in [9] derived the outage probabilities (OPs) and diversity gains for both primary and backscatter links in a PBC system under the assumption of perfect SIC at D. Considering the imperfect SIC at D and the energy-causality constraint at BD, the authors of [8] derived the OPs for both primary and backscatter links of PBC. The results in [8] and [9] indicated that the co-channel interference in PBC leads to the saturation of OPs for both primary and backscatter links, resulting in a diversity gain of zero. This issue was solved in [10] and [11], where adaptive PRC was designed to ensure the successful decoding of the primary signals. In [12], the authors investigated the scaling behavior of OP and ergodic capacity in PBC. The authors in [13] maximized the ergodic capacity of the backscatter link in PBC by optimizing the PU's transmit power and the BD's reflection coefficient, subject to the energy-causality constraint of BD. The authors in [14] maximized the sum rate of the primary and backscatter links by optimizing the PU's beamforming vector. To enhance the BD's transmission performance, the authors in [15] proposed and evaluated a reconfigurable intelligent surface (RIS) assisted PBC, in which one part of RIS is used to improve the wireless channel conditions and the remaining part is used to perform BC. The PBC was also integrated into the non-orthogonal multiple access (NOMA) system [16], where the BD modulates and reflects the composite signal of two NOMA users. The performance of the PBC-NOMA was improved by employing simultaneously transmitting and reflecting reconfigurable intelligent surface in [17], [18].

2) Related Works on MBC: The authors in [7] maximized the weighted sum rate of both the PU and BD in an MBC system by jointly optimizing the PU's transmit power and beam-

This work was supported in part by the National Natural Science Foundation of China under Grants 62201451, 62301421, and 62471388, and in part by the Innovation Capability Support Program of Shaanxi under Grant 2024ZC-KJXX-016. *(Corresponding Author: Xiaoli Chu)*

Yinghui Ye and Guangyue Lu are with the Shaanxi Key Laboratory of Information Communication Network and Security, Xi'an University of Posts & Telecommunications, Xi'an, 710121, China (e-mail:connectyyh@126.com, tonylugy@163.com).

Yujia Tian is with the Shangqiu Branch of China Mobile Communications Corporation, Shangqiu, 476000, China (e-mail: yujiatian_1998@126.com).

Xiaoli Chu is with the Department of Electronic and Electrical Engineering, The University of Sheffield, U.K. (e-mail: x.chu@sheffield.ac.uk).

Sumei Sun is with the Institute for Infocomm Research, Agency for Science, Technology and Research, Singapore (e-mail: sunsm@i2r.a-star.edu.sg).

forming vectors. Considering multiple BDs and their energy-causality constraints, the authors in [19] maximized the energy efficiency of an MBC system by jointly optimizing the PU's transmit power and the power reflection coefficient (PRC) and time of each BD. The authors in [20] derived the upper bounds of the ergodic rate for both the primary and backscatter links of an MBC system. In [21], the authors derived the bit error rate (BER) of both PU and BD's transmissions, and revealed the minimum symbol period ratio between BD and PU that is required for the BD reflected signal to help reduce the BER of the PU's transmission. Considering the hardware impairments (HIs) in an MBC system, the authors in [22] and [23] derived the rate expressions of the PU and BD, and demonstrated that even under HIs, the signal reflected by BD can still boost the PU's transmission rate. Considering the energy-causality constraint for the BD, the ergodic capacities of both primary and backscatter links were derived in closed forms in [24], [25]. Those results indicated that imposing an energy-causality constraint on the BD reduces the ergodic capacities of both primary and backscatter links. Two multiple access schemes, i.e., simultaneous access and selection diversity access, were proposed for multi-BD MBC and analyzed in term of the ergodic rate in [26].

We note the following gaps left by the above works.

- The outage performance of the MBC has been largely overlooked in the existing works, although it has been extensively studied for the PBC (see [8]–[11] and references therein).
- All of the above works on MBC [7], [19]–[26] assumed the availability of direct links between the PU/BD and D, which however may be blocked due to deep fading and/or obstacles in many application scenarios. For such scenarios, the use of relay[1] technology [27] to support the transmission from the PU/BD to D in an MBC system has not been investigated yet. The existing works on the combination of BC and relay cannot be readily applied to an MBC system because they either used a dedicated energy source to forward the BD's signal to D [28] or let a BD serve as a relay for other BD(s) but without sending its own information to D [29].
- A BD is typically capable of harvesting energy from incident signals and can potentially sustain their circuit power consumption without using battery energy, yet the energy-causality constraint of BD in MBC has been overlooked in [7], [20]–[23], [26]. Although [19], [24] and [25] considered the energy-causality constraint of BD, the resulting outage performance of MBC was not studied.

In this paper, we address the above gaps and study the outage performance of a relay-assisted MBC network, while considering the energy-causality constraint of the BD. Our main contributions are summarized as follows.

[1]It should be pointed out that the reconfigurable intelligence surface can also used to address the absence of direct links between the PU/BD and D. It will be an interesting topic of future work.

- We propose a relay-assisted MBC network, where the PU shares both the spectrum and energy resources with the energy self-sustaining BD and they both transmit information to D with the help of a decode-and-forward relay (R) due to the absence of direct links between the PU/BD and D. Since R needs to forward both signals from the BD and PU to D, the performance of the relay-assisted MBC network depends on the forwarding scheme employed at R. We propose three forwarding schemes[2] for R to address how R forwards both PU's and BD's signals to D: (i) an orthogonal time-division multiple access (OMA) scheme that allocates two equal sub-time slots to forward PU and BD's signals sequentially to D, (ii) a non-orthogonal multiple access (NOMA) with static power allocation (PA) scheme that allocates fixed power levels for conveying PU's and BD's signals to D simultaneously, and (iii) a NOMA with dynamic PA scheme that dynamically adjusts the power levels for forwarding PU's and BD's signals to minimize BD's OP, without degrading PU's OP with respect to the case that R forwards only PU's signal to D.
- We derive the OP expressions of the primary (from PU to D through R) and backscatter (from BD to D through R) links for each of the three relay forwarding schemes under Rayleigh fading channels. Based on the derived OP expressions, we show that the diversity gains of the primary and backscatter links both equal one under each of the three forwarding schemes, while their OPs are different for different forwarding schemes.
- Simulation results are provided to verify the accuracy of our analytical results and evaluate the performance of the proposed relay-assisted MBC network in comparison with a relay-assisted PBC network and a traditional decode-and-forward relay network that contains only PU, R and D. Our analytical and simulation results reveal the impact of the decode-and-forward relay on the outage performance of MBC and provide practical insights into how the PRC of the BD and the location and forwarding scheme of R should be properly set to minimize the OP of the PU or BD.

II. System Model and Forwarding Schemes

Fig. 1 shows our proposed relay-assisted MBC network, where R adopts the half-duplex decode-and-forward protocol[3] and supports both the primary link (PU$\rightarrow$R$\rightarrow$D) and the backscatter link (BD$\rightarrow$R$\rightarrow$D) with the target throughput R_1 and R_2, respectively. The BD's circuit structure can be referred to Fig. 1 of [8]. For simplicity, all the nodes are equipped

[2]The proposed three forwarding schemes can be directly applied to relay-assisted PBC, yet the outage performance may differ from that of relay-assisted MBC and require a separate study.

[3]It should be noted that adopting the full-duplex decode-and-forward protocol can nearly double spectral efficiency, as compared to the half-duplex one considered in this work.

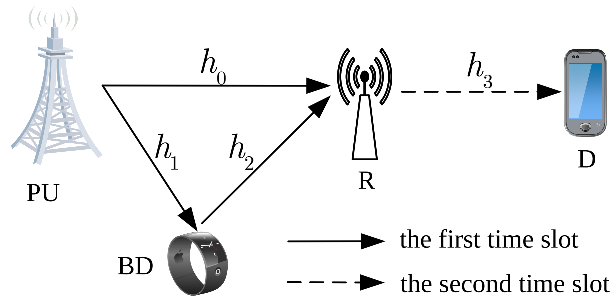

Fig. 1. System model.

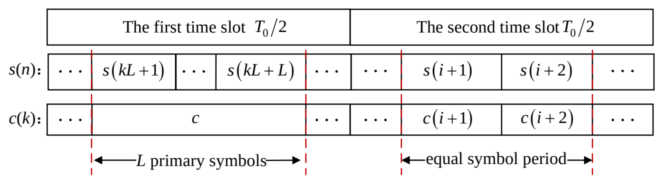

Fig. 2. Frame structure of each time slot in a two-hop relay network.

with a single antenna[4]. We assume that there are no direct links between PU/BD and D due to deep fading and/or obstacles, i.e., the communication from PU/BD to D has to rely on R. All channels are assumed to follow independent quasi-static Rayleigh fading, i.e., each channel stays static during a transmission block T_0 but may vary between adjacent transmission blocks. The channel coefficients for the links PU $\to$ R, PU $\to$ BD, BD $\to$ R, and R $\to$ D are denoted by $h_j \sim \mathcal{CN}\left(0, d_j^{-v_j}\right)$, $j = 0,1,2,3$, respectively, where v_j and d_j denote the path loss exponent and the distance of the corresponding link, respectively. Thus, the channel gain $|h_j|^2$ follows an exponential distribution with the parameter $\lambda_j = d_j^{v_j}$. As shown in Fig. 2, each transmission block T_0 is divided into two equal time slots that are allocated to the two hops respectively.

A. The First Time Slot

In the first time slot, PU sends its signal to R with transmit power $P_{\rm t}$, and BD modulates and reflects a part of the incident signal to R while harvesting energy from the remaining incident signal. Let $s(n) \sim \mathcal{CN}(0,1)$ and $c(k) \sim \mathcal{CN}(0,1)$ denote the PU's signal in the *n*-th symbol period and the BD's signal in the *k*-th symbol period, respectively. In MBC [7], [19]–[26], the symbol period of $c(k)$, denoted by $T_{\rm c}$, is L times longer than that of $s(n)$, denoted by $T_{\rm s}$, i.e., $T_{\rm c} = LT_{\rm s}$, where $L \gg 1$ is a positive integer, but T_c is much shorter than T_0.

Considering a nonlinear energy harvesting (EH) model, the harvested power $P_{\rm e}$ at BD can be written as

$$P_{\rm e} = f(P_r) \tag{1}$$

[4]We note that the spatial modulation [30] and index modulation [31] have been proposed for enhancing the BD's transmission performance. These novel modulation schemes can also be applied in our considered network if multiple antennas are adopted.

where $P_r = (1-\beta) P_{\rm t}|h_1|^2$ is the input power to the EH circuit, $\beta \in [0,1]$ is the PRC of BD, and $f(\cdot)$ is a function that describes the mapping relationship between the input power and the harvested power.

We assume that the BD is activated[5] only when the energy-causality constraint $P_{\rm e} \geq P_{\rm c}$ is satisfied, where $P_{\rm c}$ denotes the BD's circuit power consumption required for backscattering. Substituting (1) into $P_{\rm e} \geq P_{\rm c}$ and using the fact that the harvested power of a nonlinear EH model is a non-decreasing function with respect to its input power, this energy-causality constraint of the BD is equivalent to

$$|h_1|^2 \geq \frac{\phi}{(1-\beta) P_{\rm t}}, \tag{2}$$

where $\phi = f^{-1}(P_{\rm c})$, and $f^{-1}(\cdot)$ is the inverse function of the nonlinear EH model.

Remark 1: The function $f^{-1}(P_{\rm c})$ can be any nonlinear EH model, thus ensuring the applicability of our analytical framework to various nonlinear EH models.

Depending on whether $P_{\rm e} \geq P_{\rm c}$ holds or not, the received signal at R falls into one of the following two cases.

Case I : If $P_{\rm e} \geq P_{\rm c}$, BD is activated, then it modulates its own signal $c(k)$ on the incident signal $\sqrt{P_{\rm t}} h_1 s(n)$ and backscatters the modulated signal $\sqrt{P_{\rm t}\beta} h_1 c(k) s(n)$ to R. The received signal at R can be written as

$$y_{\rm r}^{(\rm I)}(n) = \sqrt{P_{\rm t}} h_0 s(n) + \sqrt{P_{\rm t}\beta} h_1 h_2 c(k) s(n) + z_{\rm r}(n), \tag{3}$$

where $z_{\rm r}(n) \sim \mathcal{CN}(0, \sigma^2)$ denotes the additive white Gaussian noise (AWGN) at R.

In this case, R first decodes $s(n)$ by treating $\sqrt{P_{\rm t}\beta} h_1 h_2 c(k) s(n)$ as a useful signal since $T_{\rm c} \gg T_{\rm s}$ and then detects $c(k)$ after using the SIC technique to subtract $\sqrt{P_{\rm t}} h_0 s(n)$ from the received signal over $LT_{\rm s}$ [7]. According to [7, eq. (11)] and [7, eq. (18)], the achievable throughput (bit) in the first hop of the primary link and the backscatter link can be expressed as, respectively,

$$R_{\rm r,s}^{(\rm I)} = \frac{BT_0}{2} \mathbb{E}_{c(k)} \left[\log_2 \left(1 + \rho \left| h_0 + \sqrt{\beta} c(k) h_1 h_2 \right|^2 \right) \right], \tag{4}$$

$$R_{\rm r,c}^{(\rm I)} = \frac{BT_0}{2L} \log_2 \left(1 + \gamma_{\rm r,c}^{(\rm I)} \right), \tag{5}$$

where $\rho = \frac{P_t}{\sigma^2}$ is the input signal-to-noise ratio (SNR), B is the bandwidth, $\rho \left| h_0 + \sqrt{\beta} c(k) h_1 h_2 \right|^2$ and $\gamma_{\rm r,c}^{(\rm I)} = \rho\beta L |h_1|^2 |h_2|^2$ are the SNR to decode BD's and PU's signals, respectively, and $\mathbb{E}_x[\cdot]$ denotes the expectation operator over the random variable x. Please note that (5) is derived under the assumption

[5]This assumption relies on the harvested power being used immediately to support the BC, which is feasible in practice for the following reasons. The circuit power consumption of BC typically ranges from several microwatts to tens of microwatts. This level of power can be effectively provided by mainstream EH receivers (e.g., Powercast's P2110/P2110B and P1110) when the distance for wireless power transfer is within a few meters. Yet, it should be noted that allowing a pure EH phase for BD to accumulate energy [32] can greatly increase the probability that the BD is activated and the OP of the backscatter link.

of perfect SIC [7], [19]–[26]. Since the main purpose of this work is to propose a relay-assisted MBC network and then to evaluate its achievable outage performance under the energy-causality constraint, perfect SIC is assumed for analytical tractability in deriving the OP expressions.

Case II : If $P_{\rm e} < P_{\rm c}$, BD does not backscatter signals to R. Then, the signal received at R is

$$y_{\rm r}^{({\rm II})}\left(n\right) = \sqrt{P_{\rm t}}h_0 s\left(n\right) + z_{\rm r}\left(n\right). \tag{6}$$

Based on (6), the achievable throughput (bit) in the first hop of the primary link is

$$R_{\rm r,s}^{({\rm II})} = \frac{BT_0}{2}\log_2\left(1+\gamma_{\rm r,s}^{({\rm II})}\right), \tag{7}$$

where $\gamma_{\rm r,s}^{({\rm II})} = \rho |h_0|^2$.

We can see that $P_{\rm e}$, $R_{\rm r,s}^{({\rm I})}$, and $R_{\rm r,c}^{({\rm I})}$ all involve the same channel coefficient h_1. This introduces coupling between the OPs of the primary and backscatter links, which would not be present if the energy-causality constraint at BD is not considered.

B. The Second Time Slot

In the second time slot, R re-encodes the decoded signals and sends them to D with transmit power $P_{\rm t}$. Here we use $\widehat{s}\left(i\right)$ and $\widehat{c}\left(i\right)$ to denote re-encoded signals of the PU and the BD, respectively, and both them follow $\mathcal{CN}\left(0,1\right)$. Depending on whether BD is activated or not and whether R successfully decodes $s\left(n\right)$ and $c\left(k\right)$ or not, the signal received by D can be one of the following three cases.

Case 1: If R fails to decode the PU's signal, R will not forward any signal to D due to the SIC order given in the previous subsection. In this case, the SNRs for decoding $\widehat{s}\left(i\right)$ and $\widehat{c}\left(i\right)$ all equal zero and both the primary and backscatter links are in outage.

Case 2: If $P_{\rm e} \geq P_{\rm c}$ and R successfully decodes $s\left(i\right)$ only, or if $P_{\rm e} < P_{\rm c}$ and $s\left(i\right)$ is successfully decoded by R, then the received signal at D can be expressed as

$$y_{\rm d}^{(2)}\left(i\right) = \sqrt{P_{\rm t}}h_3 \hat{s}\left(i\right) + z_{\rm d}\left(i\right), \tag{8}$$

where $z_{\rm d}\left(i\right) \sim \mathcal{CN}\left(0,\sigma^2\right)$ denotes the AWGN at D. Then, the throughput (bit) of the primary link, in the second hop, is

$$R_{\rm d,s}^{(2)} = \frac{BT_0}{2}\log_2\left(1+\gamma_{\rm d,s}^{(2)}\right). \tag{9}$$

In this case, the SNRs for decoding $\widehat{s}\left(i\right)$ and $\widehat{c}\left(i\right)$ are $\gamma_{\rm d,s}^{(2)} = \rho |h_3|^2$ and zero, respectively. Therefore, the PU's signal may be decoded at D while the backscatter link experiences outage.

Case 3: If $P_{\rm e} \geq P_{\rm c}$ and R successfully decodes both the PU's signal and the BD's signal, then R will forward the signals $\widehat{s}\left(i\right)$ and $\widehat{c}\left(i\right)$ to D. In this case, we propose three forwarding schemes at R, i.e., OMA scheme, NOMA with static PA scheme, and NOMA with dynamic PA scheme.

1) OMA Scheme: In this scheme, the second time slot is further divided into two equal sub-time slots, which are used by R to transmit the signals of PU and BD respectively. In the first and second sub-time slots, the signals received by D can be, respectively, represented as

$$y_{\rm d,s}^{\rm OMA}\left(i\right) = \sqrt{P_{\rm t}}h_3 \hat{s}\left(i\right) + z_{\rm d}\left(i\right), \tag{10}$$

$$y_{\rm d,c}^{\rm OMA}\left(i\right) = \sqrt{P_{\rm t}}h_3 \hat{c}\left(i\right) + z_{\rm d}\left(i\right). \tag{11}$$

Then, the achievable throughput (bit) for the primary and backscatter links can be respectively expressed as

$$R_{\rm d,s}^{\rm OMA} = \frac{BT_0}{4}\log_2\left(1+\gamma_{\rm d,s}^{\rm OMA}\right), \tag{12}$$

$$R_{\rm d,c}^{\rm OMA} = \frac{BT_0}{4}\log_2\left(1+\gamma_{\rm d,c}^{\rm OMA}\right), \tag{13}$$

where $\gamma_{\rm d,s}^{\rm OMA}\rho |h_3|^2$ and $\gamma_{\rm d,c}^{\rm OMA} = \rho |h_3|^2$ are the SNRs for decoding $\widehat{s}\left(i\right)$ and $\widehat{c}\left(i\right)$, respectively.

2) NOMA with Static PA Scheme: In this scheme, R transmits the composite signal $\sqrt{a_1^{\rm ST}}\hat{s}\left(i\right) + \sqrt{a_2^{\rm ST}}\hat{c}\left(i\right)$ to D via NOMA [6], where $a_1^{\rm ST}$ and $a_2^{\rm ST}$ are the nonnegative static PA factors and satisfy $a_1^{\rm ST} + a_2^{\rm ST} = 1$. Here, the superscript 'ST' stands for 'static', and $a_1^{\rm ST}$ and $a_2^{\rm ST}$ keep constant[7] for all transmission blocks. Accordingly, the signal received at D is

$$y_{\rm d}^{\rm ST}\left(i\right) = \sqrt{P_{\rm t}}h_3\left(\sqrt{a_1^{\rm ST}}\hat{s}\left(i\right) + \sqrt{a_2^{\rm ST}}\hat{c}\left(i\right)\right) + z_{\rm d}\left(i\right). \tag{14}$$

Upon receiving $y_{\rm d}^{\rm ST}\left(i\right)$, D first decodes $\widehat{s}\left(i\right)$ by treating $\widehat{c}\left(i\right)$ as interference, and then detects $\widehat{c}\left(i\right)$ by using SIC technique [34]. Assuming perfect SIC, the achievable throughput (bit) of the primary link and the backscatter link, in the second hop, can be written as, respectively,

$$R_{\rm d,s}^{\rm ST} = \frac{BT_0}{2}\log_2\left(1+\gamma_{\rm d,s}^{\rm ST}\right), \tag{15}$$

$$R_{\rm d,c}^{\rm ST} = \frac{BT_0}{2}\log_2\left(1+\gamma_{\rm d,c}^{\rm ST}\right), \tag{16}$$

where $\gamma_{\rm d,s}^{\rm ST} = \frac{P_{\rm t} a_1^{\rm ST}|h_3|^2}{P_{\rm t} a_2^{\rm ST}|h_3|^2+\sigma^2}$ and $\gamma_{\rm d,c}^{\rm ST} = \rho a_2^{\rm ST}|h_3|^2$ are the SINR/SNR for decoding $\widehat{s}\left(i\right)$ and $\widehat{c}\left(i\right)$, respectively.

[6] Although such an approach is similar to rate splitting (RS), there exists a difference. In RS, it is crucial to design an RS coefficient, which should be adaptively adjusted according to wireless channel conditions and determines the target throughput of $\hat{s}\left(i\right)$ and $\hat{c}\left(i\right)$ [33]. However, in this work, the target throughput of $\hat{s}\left(i\right)$ and $\hat{c}\left(i\right)$ is fixed at R_1 and R_2, respectively, and hence RS is not suitable.

[7] The values of $a_1^{\rm ST}$ and $a_2^{\rm ST}$ can be determined empirically or analytically, e.g., based on the PU and BD's OPs that will be derived as a function of $a_1^{\rm ST}$ and $a_2^{\rm ST}$ in the following sections.

3) NOMA with Dynamic PA Scheme: In this scheme, R transmits the composite signal $\sqrt{a_1^{\mathrm{DY}}}\hat{s}(i)+\sqrt{a_2^{\mathrm{DY}}}\hat{c}(i)$ to D, where a_1^{DY} and a_2^{DY} are the nonnegative dynamic PA factors with the superscript 'DY' denoting 'dynamic', $a_1^{\mathrm{DY}}+a_2^{\mathrm{DY}}=1$, and both a_1^{DY} and a_2^{DY} vary with the change of channel coefficient of h_3. The signal received by D can be written as

$$y_{\mathrm{d}}^{\mathrm{DY}}(i)=\sqrt{P_{\mathrm{t}}}h_3\left(\sqrt{a_1^{\mathrm{DY}}}\hat{s}(i)+\sqrt{a_2^{\mathrm{DY}}}\hat{c}(i)\right)+z_{\mathrm{d}}(i). \quad (17)$$

Then, following the same SIC order as adopted in the NOMA with static PA scheme, the achievable throughput (bit) of the primary and backscatter links can be expressed as, respectively,

$$R_{\mathrm{d,s}}^{\mathrm{DY}}=\frac{BT_0}{2}\log_2\left(1+\gamma_{\mathrm{d,s}}^{\mathrm{DY}}\right), \quad (18)$$

$$R_{\mathrm{d,c}}^{\mathrm{DY}}=\frac{BT_0}{2}\log_2\left(1+\gamma_{\mathrm{d,c}}^{\mathrm{DY}}\right), \quad (19)$$

where $\gamma_{\mathrm{d,s}}^{\mathrm{DY}}=\frac{P_{\mathrm{t}}a_1^{\mathrm{DY}}|h_3|^2}{P_{\mathrm{t}}a_2^{\mathrm{DY}}|h_3|^2+\sigma^2}$ and $\gamma_{\mathrm{d,c}}^{\mathrm{DY}}=\rho a_2^{\mathrm{DY}}|h_3|^2$ are the SINR/SNR for decoding $\widehat{s}(i)$ and $\widehat{c}(i)$, respectively.

In the NOMA with dynamic PA scheme, the dynamic PA factors are optimized to minimize BD's OP while ensuring that the PU's OP does not fall below that of the case of R forwarding only PU's signal to D. To obtain the optimal dynamic PA factors, we provide the following Lemmas.

Lemma 1. If $|h_3|^2\geq\frac{\gamma_1+\gamma_2+\gamma_1\gamma_2}{\rho}$, then the optimal a_1^{DY}, denoted by $a_1^{\mathrm{DY}*}$, can be any value in the interval $\left[\frac{P_{\mathrm{t}}\gamma_1|h_3|^2+\gamma_1\sigma^2}{P_{\mathrm{t}}|h_3|^2+P_{\mathrm{t}}\gamma_1|h_3|^2},1-\frac{\gamma_2\sigma^2}{P_{\mathrm{t}}|h_3|^2}\right]$, and the optimal a_2^{DY}, denoted by $a_2^{\mathrm{DY}*}$, is given by $a_2^{\mathrm{DY}*}=1-a_1^{\mathrm{DY}*}$, where $\gamma_1=2^{\frac{2R_1}{BT_0}}-1$ and $\gamma_2=2^{\frac{2LR_2}{BT_0}}-1$ represent the minimum signal-to-interference-plus-noise ratio (SINR) required for decoding the PU and BD's signals, respectively, and D can successfully decode the information of both PU and BD. If $|h_3|^2<\frac{\gamma_1+\gamma_2+\gamma_1\gamma_2}{\rho}$, then we have $a_1^{\mathrm{DY}*}=1$ and $a_2^{\mathrm{DY}*}=0$, i.e., R forwards only the PU's signal to D and the backscattered link is in outage.

Proof. Please refer to Appendix A. ■

Remark 2: Lemma 1 highlights the following three properties of the NOMA with dynamic PA scheme. First, whether or not R forwards the BD's signal depends on h_3 and the target throughput of both PU and BD. Specifically, if $|h_3|^2\geq\frac{\gamma_1+\gamma_2+\gamma_1\gamma_2}{\rho}$, then R forwards both PU and BD's signals to D and the outage performance of the R $\rightarrow$ D link under the NOMA with optimal dynamic PA is the same as that of the scenario where only PU's signal is forwarded. If $|h_3|^2<\frac{\gamma_1+\gamma_2+\gamma_1\gamma_2}{\rho}$, allowing R to forward BD's signal not only leads to an outage event of the backscatter link, but also degrades the PU's outage performance. In such a case, the optimal choice for R is to forward only PU's signal. Second, in the relay-assisted MBC, under the NOMA with optimal dynamic PA, the backscatter link enhances the PU's outage performance due to the following two reasons. In the first time slot, the BD $\rightarrow$ R link increases the throughput of the PU $\rightarrow$ R link, decreasing the probability that R fails to decode PU's signal. While in the second time slot, the dynamic PA can ensure that the PU's outage performance is maintained the same as in the scenario where only PU's signal is forwarded. Third, a higher target throughput of the BD increases the probability that the BD's signal is not forwarded by R, thus degrading the BD's outage performance. This issue can be alleviated by positioning R relatively closer to D such that the probability of satisfying $|h_3|^2\geq\frac{\gamma_1+\gamma_2+\gamma_1\gamma_2}{\rho}$ increases while maintaining sufficiently good h_0, h_1, and h_2 for R to decode signals of both PU and BD..

For $|h_3|^2<\frac{\gamma_1+\gamma_2+\gamma_1\gamma_2}{\rho}$, the PU's outage performance in the second time slot under the NOMA with dynamic PA scheme is summarized by Lemma 1.

Lemma 2. For $\frac{\gamma_1}{\rho}\leq|h_3|^2<\frac{\gamma_1+\gamma_2+\gamma_1\gamma_2}{\rho}$, R forwards only the PU's signal to D with $a_1^{\mathrm{DY}*}=1$ and D can successfully decode the re-encoded PU's signal $\hat{s}(i)$. However, for $|h_3|^2<\frac{\gamma_1}{\rho}$, R does not forward the PU's signal to D because D will not be able to decode the PU's signal. In this case, R keeps silent[8] and we have $a_1^{\mathrm{DY}*}=a_2^{\mathrm{DY}*}=0$.

Proof. If $|h_3|^2<\frac{\gamma_1+\gamma_2+\gamma_1\gamma_2}{\rho}$, R only forwards the PU's signal. In this case, to ensure the success of decoding $\widehat{s}(i)$, $R_{\mathrm{d,s}}^{\mathrm{DY}}=\frac{BT_0}{2}\log_2\left(1+\frac{P_{\mathrm{t}}|h_3|^2}{\sigma^2}\right)\geq R_1$ should be satisfied. Thus, $\widehat{s}(i)$ can be successfully decoded by D if and only if $\rho|h_3|^2\geq\gamma_1$ is satisfied. The proof is complete. ■

Based on Lemmas 1 and 2, the optimal a_1^{DY} and a_2^{DY} can be summarized below:

$$\begin{cases} a_1^{\mathrm{DY}*}\in\left[\frac{P_{\mathrm{t}}\gamma_1|h_3|^2+\gamma_1\sigma^2}{P_{\mathrm{t}}|h_3|^2+P_{\mathrm{t}}\gamma_1|h_3|^2},1-\frac{\gamma_2\sigma^2}{P_{\mathrm{t}}|h_3|^2}\right], & \\ \text{and } \mathrm{a}_2^{\mathrm{DY}*}=1-\mathrm{a}_1^{\mathrm{DY}*}, & \text{if } |\mathrm{h}_3|^2\geq\frac{\gamma_1+\gamma_2+\gamma_1\gamma_2}{\rho} \\ a_1^{\mathrm{DY}*}=1, a_2^{\mathrm{DY}*}=0, & \text{if } \frac{\gamma_1}{\rho}\leq|h_3|^2<\frac{\gamma_1+\gamma_2+\gamma_1\gamma_2}{\rho} \\ a_1^{\mathrm{DY}*}=a_2^{\mathrm{DY}*}=0, & \text{if } |h_3|^2<\frac{\gamma_1}{\rho} \end{cases}. \quad (20)$$

III. Outage Analysis for Primary Link

In this section, we derive the OP and diversity gain of the primary link under the three proposed relay forwarding schemes.

A. OMA Scheme

An outage event occurs when the throughput of either hop falls below the target. Thus, the primary link's OP is written

[8] We note that allowing R to forward BD's signal only when $\frac{\gamma_2}{\rho}\leq|h_3|^2<\frac{\gamma_1}{\rho}$ can further reduce the BD's OP. This consideration is not allowed in the current system because D adopts a fixed SIC order in the second time slot, where the PU's and BD's signals are decoded sequentially. If it is allowed in the NOMA with dynamic PA scheme, then the first decoded signal at D will be from BD when $\frac{\gamma_2}{\rho}\leq|h_3|^2<\frac{\gamma_1}{\rho}$, whereas it will be from PU when $|h_3|^2\geq\frac{\gamma_1}{\rho}$. Thus, for D to know whether the first decoded signal is from PU or BD, R would need to inform D accordingly in each second time slot, which introduces additional overhead.

as

$$
\begin{aligned}
P_{\mathrm{p,out}}^{\mathrm{OMA}} =& 1-\Pr\left(P_{\mathrm{e}}\geq P_{\mathrm{c}}, R_{\mathrm{r,s}}^{(\mathrm{I})}\geq R_1, R_{\mathrm{r,c}}^{(\mathrm{I})}\geq R_2, R_{\mathrm{d,s}}^{\mathrm{OMA}}\geq R_1\right)\\
&-\Pr\left(P_{\mathrm{e}}\geq P_{\mathrm{c}}, R_{\mathrm{r,s}}^{(\mathrm{I})}\geq R_1, R_{\mathrm{r,c}}^{(\mathrm{I})}< R_2, R_{\mathrm{d,s}}^{(2)}\geq R_1\right)\\
&-\Pr\left(P_{\mathrm{e}}< P_{\mathrm{c}}, R_{\mathrm{r,s}}^{(\mathrm{II})}\geq R_1, R_{\mathrm{d,s}}^{(2)}\geq R_1\right)\\
\overset{(a)}{\geq}& 1-\underbrace{\Pr\left(P_{\mathrm{e}}\geq P_{\mathrm{c}}, \gamma_{\mathrm{r,s}}^{(\mathrm{I})}\geq \gamma_1, \gamma_{\mathrm{r,c}}^{(\mathrm{I})}\geq \gamma_2\right)}_{P_{\mathrm{p,1}}^{\mathrm{OMA}}}\underbrace{\Pr\left(\gamma_{\mathrm{d,s}}^{\mathrm{OMA}}\geq \gamma_1^{\mathrm{OMA}}\right)}_{P_{\mathrm{p,2}}^{\mathrm{OMA}}}\\
&-\underbrace{\Pr\left(P_{\mathrm{e}}\geq P_{\mathrm{c}}, \gamma_{\mathrm{r,s}}^{(\mathrm{I})}\geq \gamma_1, \gamma_{\mathrm{r,c}}^{(\mathrm{I})}< \gamma_2\right)}_{P_{\mathrm{p,3}}^{\mathrm{OMA}}}\underbrace{\Pr\left(\gamma_{\mathrm{d,s}}^{(2)}\geq \gamma_1\right)}_{P_{\mathrm{p,4}}^{\mathrm{OMA}}}\\
&-\underbrace{\Pr\left(P_{\mathrm{e}}< P_{\mathrm{c}}, \gamma_{\mathrm{r,s}}^{(\mathrm{II})}\geq \gamma_1\right)}_{P_{\mathrm{p,5}}^{\mathrm{OMA}}}P_{\mathrm{p,4}}^{\mathrm{OMA}}.
\end{aligned}
\tag{21}
$$

In (21), $\gamma_1^{\mathrm{OMA}} = 2^{\frac{4R_1}{BT_0}}-1$, step (a) is obtained by applying Jensen's Inequality, which is tight since there is no co-channel interference and the input SNR is high., i.e., $\mathbb{E}_{c(k)}\left[\log_2\left(1+\rho\left|h_0+\sqrt{\beta}c\left(k\right)h_1h_2\right|^2\right)\right] \leq \log_2\left(1+\rho\mathbb{E}_{c(k)}\left|h_0+\sqrt{\beta}c\left(k\right)h_1h_2\right|^2\right) = \log_2\left(1+\gamma_{\mathrm{r,s}}^{(\mathrm{I})}\right)$, where $\gamma_{\mathrm{r,s}}^{(\mathrm{I})}=\rho\left(|h_0|^2+\beta|h_1|^2|h_2|^2\right)$, and the equality holds due to $\mathbb{E}_{c(k)}\left[\sqrt{\beta}c\left(k\right)h_0h_1h_2\right] = 0$ in one transmission block. It can be observed from (21) that P_{e}, $R_{\mathrm{r,s}}^{(\mathrm{I})}$, and $R_{\mathrm{r,c}}^{(\mathrm{I})}$ involves the channel coefficient from PU to BD h_1. This introduces extra coupling in $P_{\mathrm{p,1}}^{\mathrm{OMA}}$ and $P_{\mathrm{p,3}}^{\mathrm{OMA}}$ compared to that without considering the energy-causality constraint. The same observation also exists in deriving OP of the backscatter link.

In what follows, we derive $P_{\mathrm{p,1}}^{\mathrm{OMA}}$, $P_{\mathrm{p,2}}^{\mathrm{OMA}}$, $P_{\mathrm{p,3}}^{\mathrm{OMA}}$, $P_{\mathrm{p,4}}^{\mathrm{OMA}}$ and $P_{\mathrm{p,5}}^{\mathrm{OMA}}$ in closed forms.

1) Derivation of $P_{\mathrm{p,1}}^{\mathrm{OMA}}$ and $P_{\mathrm{p,3}}^{\mathrm{OMA}}$: The approximations of $P_{\mathrm{p,1}}^{\mathrm{OMA}}$ and $P_{\mathrm{p,3}}^{\mathrm{OMA}}$ are summarized below.

Proposition 1. $P_{\mathrm{p,1}}^{\mathrm{OMA}}$ can be approximated by (22), as shown at the top of the next page, where $b_1 = \frac{\phi}{(1-\beta)P_{\mathrm{t}}}$, $b_2 = \gamma_1\rho^{-1}$, $b_3 = \frac{\gamma_2}{\rho\beta L}$, $b_4 = b_2-\beta b_3$, $b_5 = \beta\lambda_1\lambda_0 e^{-\lambda_0 b_2}$, $b_6 = \frac{\beta\phi\lambda_0}{\beta\phi\lambda_0-\lambda_2(1-\beta)P_{\mathrm{t}}}$, $d_m = \frac{b_3(c_m+1)}{2b_1}$, $\theta_m = \frac{\pi-2\arctan b_1}{4}\cos\left(\frac{2m-1}{2M}\pi\right)+\frac{\pi+2\arctan b_1}{4}$, $c_m = \cos\left(\frac{2m-1}{2M}\pi\right)$, $w=\frac{\pi}{M}$, and M is a complexity-accuracy tradeoff parameter.

Proof. Please refer to Appendix B. ■

Proposition 2. $P_{\mathrm{p,3}}^{\mathrm{OMA}}$ can be approximated as (24), as shown at the top of the next page, where $g_m = \lambda_0 - \frac{\lambda_2(c_m+1)}{2\beta b_1}$, $u_m = \frac{b_3(c_m+1)}{2b_1}$, $r_m = \frac{b_3(c_m+1)}{2b_1}$.

Proof. Please refer to Appendix C. ■

2) Derivation of $P_{\mathrm{p,2}}^{\mathrm{OMA}}$: Substituting $\gamma_{\mathrm{d,s}}^{\mathrm{OMA}}=\rho|h_3|^2$ into $P_{\mathrm{p,2}}^{\mathrm{OMA}}$, we have

$$
\begin{aligned}
P_{\mathrm{p,2}}^{\mathrm{OMA}} &= \Pr\left(\rho|h_3|^2\geq\gamma_1^{\mathrm{OMA}}\right)\\
&= \int_{\gamma_1^{\mathrm{OMA}}\rho^{-1}}^{\infty} f_{|h_3|^2}\left(x\right)dx = e^{-\lambda_3\gamma_1^{\mathrm{OMA}}\rho^{-1}}.
\end{aligned}
\tag{23}
$$

3) Derivation of $P_{\mathrm{p,4}}^{\mathrm{OMA}}$: Since $\gamma_{\mathrm{d,s}}^{(2)}=\rho|h_3|^2$, $P_{\mathrm{p,4}}^{\mathrm{OMA}}$ can be calculated as

$$
\begin{aligned}
P_{\mathrm{p,4}}^{\mathrm{OMA}} &= \Pr\left(\rho|h_3|^2\geq\gamma_1\right)\\
&= \int_{\gamma_1\rho^{-1}}^{\infty} f_{|h_3|^2}\left(x\right)dx = e^{-\lambda_3\gamma_1\rho^{-1}}.
\end{aligned}
\tag{25}
$$

4) Derivation of $P_{\mathrm{p,5}}^{\mathrm{OMA}}$: Since $|h_0|^2$ and $|h_1|^2$ are independent random variables, $P_{\mathrm{p,5}}^{\mathrm{OMA}}$ is calculated as

$$
\begin{aligned}
P_{\mathrm{p,5}}^{\mathrm{OMA}} &= \Pr\left(|h_1|^2<b_1, |h_0|^2\geq b_2\right)\\
&= \int_0^{b_1}\int_{b_2}^{\infty} f_{|h_0|^2}\left(x\right)f_{|h_1|^2}\left(y\right)dxdy\\
&= e^{-\lambda_0 b_2}\left(1-e^{-\lambda_1 b_1}\right).
\end{aligned}
\tag{26}
$$

Substituting (22)-(26) into (21), the primary link's OP can be obtained as

$$
P_{\mathrm{p,out}}^{\mathrm{OMA}} \simeq 1-P_{\mathrm{p,1}}^{\mathrm{OMA}}P_{\mathrm{p,2}}^{\mathrm{OMA}}-P_{\mathrm{p,4}}^{\mathrm{OMA}}\left(P_{\mathrm{p,3}}^{\mathrm{OMA}}+P_{\mathrm{p,5}}^{\mathrm{OMA}}\right). \tag{27}
$$

B. NOMA with Static PA Scheme

Similar to (21), after applying Jason's inequality, the primary link's OP under the NOMA with static PA scheme can be expressed as

$$
\begin{aligned}
P_{\mathrm{p,out}}^{\mathrm{ST}} \geq& 1-\underbrace{\Pr\left(P_{\mathrm{e}}\geq P_{\mathrm{c}}, \gamma_{\mathrm{r,s}}^{(\mathrm{I})}\geq \gamma_1, \gamma_{\mathrm{r,c}}^{(\mathrm{I})}\geq \gamma_2\right)}_{P_{\mathrm{p,1}}^{\mathrm{ST}}}\underbrace{\Pr\left(\gamma_{\mathrm{d,s}}^{\mathrm{ST}}\geq \gamma_1\right)}_{P_{\mathrm{p,2}}^{\mathrm{ST}}}\\
&-\underbrace{\Pr\left(P_{\mathrm{e}}\geq P_{\mathrm{c}}, \gamma_{\mathrm{r,s}}^{(\mathrm{I})}\geq \gamma_1, \gamma_{\mathrm{r,c}}^{(\mathrm{I})}< \gamma_2\right)}_{P_{\mathrm{p,3}}^{\mathrm{ST}}}\underbrace{\Pr\left(\gamma_{\mathrm{d,s}}^{(2)}\geq \gamma_1\right)}_{P_{\mathrm{p,4}}^{\mathrm{ST}}}\\
&-\underbrace{\Pr\left(P_{\mathrm{e}}< P_{\mathrm{c}}, \gamma_{\mathrm{r,s}}^{(\mathrm{II})}\geq \gamma_1\right)}_{P_{\mathrm{p,5}}^{\mathrm{ST}}}P_{\mathrm{p,4}}^{\mathrm{ST}},
\end{aligned}
\tag{28}
$$

Comparing (28) with (21), we find that $P_{\mathrm{p,1}}^{\mathrm{ST}}=P_{\mathrm{p,1}}^{\mathrm{OMA}}$, $P_{\mathrm{p,3}}^{\mathrm{ST}}=P_{\mathrm{p,3}}^{\mathrm{OMA}}$, $P_{\mathrm{p,4}}^{\mathrm{ST}}=P_{\mathrm{p,4}}^{\mathrm{OMA}}$ and $P_{\mathrm{p,5}}^{\mathrm{ST}}=P_{\mathrm{p,5}}^{\mathrm{OMA}}$. Therefore, we only need to derive $P_{\mathrm{p,2}}^{\mathrm{ST}}$ as follows,

$$
\begin{aligned}
P_{\mathrm{p,2}}^{\mathrm{ST}} &= \Pr\left(\frac{\rho a_1^{\mathrm{ST}}|h_3|^2}{\rho a_2^{\mathrm{ST}}|h_3|^2+1}\geq\gamma_1\right)\\
&= \int_{\frac{\gamma_1}{\rho a_1^{\mathrm{ST}}-\rho a_2^{\mathrm{ST}}\gamma_1}}^{\infty} f_{|h_3|^2}\left(x\right)dx = e^{-\frac{\lambda_3\gamma_1}{\rho a_1^{\mathrm{ST}}-\rho a_2^{\mathrm{ST}}\gamma_1}},
\end{aligned}
\tag{29}
$$

where the second equality holds from $a_1^{\mathrm{ST}}>a_2^{\mathrm{ST}}\gamma_1$. Please note that $P_{\mathrm{p,2}}^{\mathrm{ST}}=1$ holds for $a_1^{\mathrm{ST}}\leq a_2^{\mathrm{ST}}\gamma_1$. This indicates that for the NOMA with static PA, the $a_1^{\mathrm{ST}}>a_2^{\mathrm{ST}}\gamma_1$ should be satisfied.

Then, the closed-form expression for the primary link's OP under the NOMA with static PA scheme can be obtained as

$$
P_{\mathrm{p,out}}^{\mathrm{ST}} \simeq 1-P_{\mathrm{p,1}}^{\mathrm{OMA}}P_{\mathrm{p,2}}^{\mathrm{ST}}-P_{\mathrm{p,4}}^{\mathrm{OMA}}\left(P_{\mathrm{p,3}}^{\mathrm{OMA}}+P_{\mathrm{p,5}}^{\mathrm{OMA}}\right). \tag{30}
$$

$$P_{\rm p,1}^{\rm OMA}=\frac{1}{4}\beta\lambda_1\lambda_0 e^{-\lambda_0 b_2}\left(\pi-2\arctan b_1\right)\sum_{m=1}^{M} w\sqrt{1-c_m^2}\frac{\tan\theta_m \sec^2\theta_m e^{-\lambda_1\tan\theta_m}}{\beta\lambda_0\tan\theta_m-\lambda_2}\left(e^{\left(\lambda_0-\frac{\lambda_2}{\beta\tan\theta_m}\right)b_2}-e^{\left(\lambda_0-\frac{\lambda_2}{\beta\tan\theta_m}\right)\frac{\gamma_2}{\rho L}}\right)$$
$$+b_6 e^{-\lambda_1 b_1}\left(e^{\left(\lambda_0-\frac{\lambda_2}{b_1\beta}\right)\frac{\gamma_2}{\rho L}-\lambda_0 b_2}-e^{b_4\left(\frac{\lambda_2}{b_1\beta}-\lambda_0\right)-\frac{\lambda_2 b_2}{b_1\beta}}\right)+\frac{\lambda_2 b_3}{2b_1}e^{-\lambda_0 b_4}\sum_{m=1}^{M} w\sqrt{1-c_m^2}e^{-\lambda_2 d_m-\frac{\lambda_1 b_3}{d_m}}+e^{-\lambda_1 b_1-\frac{\lambda_3 b_3}{b_1}-\lambda_0 b_4}. \quad (22)$$

$$P_{\rm p,3}^{\rm OMA}=\frac{\lambda_0\lambda_2}{2\beta b_1}e^{-\lambda_0 b_2}\sum_{m=1}^{M} w\sqrt{1-c_m^2}e^{-\frac{2\lambda_1 b_1}{(1+c_m)}}\left(e^{\beta b_3 g_m}\left(\frac{\beta b_3}{g_m}-\frac{1}{g_m^2}\right)+\frac{1}{g_m^2}\right)+\lambda_2 e^{-\lambda_0 b_2}\frac{e^{-\lambda_1 b_1}}{\lambda_0\beta b_1-\lambda_2}\left(e^{(\lambda_0\beta b_1-\lambda_2)\frac{b_3}{b_1}}-1\right)$$
$$-\frac{\lambda_2 b_3 e^{-\lambda_0 b_2}}{2b_1}\sum_{m=1}^{M} w\sqrt{1-c_m^2}\left(e^{-\lambda_2 u_m-\lambda_1\frac{b_3}{u_m}}\left(e^{\beta\lambda_0 b_3}-e^{\beta\lambda_0 b_1 u_m}\right)+e^{\lambda_0\beta b_1 r_m-\lambda_2 r_m-\lambda_1\frac{b_3}{r_m}}\right). \quad (24)$$

C. NOMA with Dynamic PA Scheme

In this scheme, D can successfully decode the PU's signal forwarded by R for $|h_3|^2 \geq \frac{\gamma_1}{\rho}$; otherwise, the primary link experiences an outage. Therefore, the OP of the primary link under this scheme can be written as

$$P_{\rm p,out}^{\rm DY} \geq 1-\underbrace{\Pr\left(P_{\rm e}\geq P_{\rm c}, \gamma_{\rm r,s}^{\rm (I)}\geq\gamma_1, \gamma_{\rm r,c}^{\rm (I)}\geq\gamma_2\right)}_{P_{\rm p,1}^{\rm DY}}\underbrace{\Pr\left(|h_3|^2\geq\frac{\gamma_1}{\rho}\right)}_{P_{\rm p,2}^{\rm DY}}$$
$$-\underbrace{\Pr\left(P_{\rm e}\geq P_{\rm c}, \gamma_{\rm r,s}^{\rm (I)}\geq\gamma_1, \gamma_{\rm r,c}^{\rm (I)}<\gamma_2\right)}_{P_{\rm p,3}^{\rm DY}}\underbrace{\Pr\left(\gamma_{\rm d,s}^{(2)}\geq\gamma_1\right)}_{P_{\rm p,4}^{\rm DY}}$$
$$-\underbrace{\Pr\left(P_{\rm e}<P_{\rm c}, \gamma_{\rm r,s}^{\rm (II)}\geq\gamma_1\right)}_{P_{\rm p,5}^{\rm DY}}P_{\rm p,4}^{\rm DY}. \quad (31)$$

Comparing (31) with (21), it is found that $P_{\rm p,1}^{\rm DY}=P_{\rm p,1}^{\rm OMA}$, $P_{\rm p,2}^{\rm DY}=P_{\rm p,4}^{\rm OMA}$, $P_{\rm p,3}^{\rm DY}=P_{\rm p,3}^{\rm OMA}$, $P_{\rm p,4}^{\rm DY}=P_{\rm p,4}^{\rm OMA}$ and $P_{\rm p,5}^{\rm DY}=P_{\rm p,5}^{\rm OMA}$. Therefore, the closed-form expression for the primary link's OP in this forwarding scheme is given by

$$P_{\rm p,out}^{\rm DY}\simeq 1-P_{\rm p,4}^{\rm OMA}\left(P_{\rm p,1}^{\rm OMA}+P_{\rm p,3}^{\rm OMA}+P_{\rm p,5}^{\rm OMA}\right). \quad (32)$$

D. Diversity Order

Based on the obtained expressions of the primary link's OP under the three forwarding schemes, we proceed to derive the diversity orders of the primary link. The diversity order [35] is defined as

$$d=-\lim_{\rho\to\infty}\frac{\lg\left(P_{\rm out}\right)}{\lg\left(\rho\right)}, \quad (33)$$

where $P_{\rm out}$ is the OP.

When $\rho\to\infty$, $P_{\rm p,out}^{\rm OMA}$, $P_{\rm p,out}^{\rm ST}$ and $P_{\rm p,out}^{\rm DY}$ depend on $Q_{22}=e^{\left(-\lambda_1 b_1-\frac{\lambda_2 b_3}{b_1}-\lambda_0 b_4\right)}$, as shown in (B.2). Since $Q_{22}\propto e^{-\frac{1}{\rho}}$ as $\rho\to\infty$, $P_{\rm p,out}^{\rm OMA}$, $P_{\rm p,out}^{\rm ST}$ and $P_{\rm p,out}^{\rm DY}\propto 1-e^{-\frac{1}{\rho}}$, where $\propto$ denotes being proportional to a certain quantity. Accordingly, the diversity orders of the primary link under the three forwarding schemes can be calculated as

$$d_{\rm p}^{\rm OMA}=d_{\rm p}^{\rm ST}=d_{\rm p}^{\rm DY}=-\lim_{\rho\to\infty}\frac{\lg\left(1-e^{-\frac{1}{\rho}}\right)}{\lg\left(\rho\right)}=1. \quad (34)$$

Remark 3: Under the three forwarding schemes, the primary link achieves the same diversity order but the achievable outage performance varies. Particularly, by comparing (32) with (30) and (27), it is not hard to verify that $P_{\rm p,out}^{\rm DY}<P_{\rm p,out}^{\rm ST}$ and $P_{\rm p,out}^{\rm DY}<P_{\rm p,out}^{\rm OMA}$ due to $P_{\rm p,4}^{\rm OMA}>P_{\rm p,2}^{\rm ST}$ and $P_{\rm p,4}^{\rm OMA}>P_{\rm p,2}^{\rm OMA}$. That is, NOMA with dynamic PA achieves the best outage performance of the PU among three forwarding schemes.

IV. Outage Analysis for Backscatter Link

The BD's signal $c(k)$ can be successfully decoded by D when the following three conditions are satisfied: 1) the BD is activated; 2) R can decode both PU and BD's signals; 3) D can decode both PU's and BD's signal. Accordingly, we derive the BD's OP under the proposed three forwarding schemes in the following.

A. OMA Scheme

In the OMA scheme, the backscatter link's OP is written as

$$P_{\rm b,out}^{\rm OMA}=1-\Pr\left(P_{\rm e}\geq P_{\rm c}, R_{\rm r,s}^{\rm (I)}\geq R_1, R_{\rm r,c}^{\rm (I)}\geq R, R_{\rm d,c}^{\rm OMA}\geq R_2\right)$$
$$=1-\underbrace{\Pr\left(P_{\rm e}\geq P_{\rm c}, \gamma_{\rm r,s}^{\rm (I)}\geq\gamma_1, \gamma_{\rm r,c}^{\rm (I)}\geq\gamma_2\right)}_{P_{\rm b,1}^{\rm OMA}}$$
$$\times\underbrace{\Pr\left(\gamma_{\rm d,c}^{\rm OMA}\geq\gamma_2^{\rm OMA}\right)}_{P_{\rm b,2}^{\rm OMA}}, \quad (35)$$

where $\gamma_2^{\rm OMA}=2^{\frac{4R_2}{BT_0}}-1$.

By comparing (35) with (21), we find that $P_{\rm b,1}^{\rm OMA}=P_{\rm p,1}^{\rm OMA}$. Thus, we only need to calculate $P_{\rm b,2}^{\rm OMA}$. By substituting $\gamma_{\rm d,c}^{\rm OMA}=\rho|h_3|^2$ into $P_{\rm b,2}^{\rm OMA}$, we have

$$P_{\rm b,2}^{\rm OMA}=\Pr\left(|h_3|^2\geq\rho^{-1}\gamma_2^{\rm OMA}\right)$$
$$=\int_{\rho^{-1}\gamma_2^{\rm OMA}}^{\infty} f_{|h_3|^2}(x)\,dx=e^{-\lambda_3\rho^{-1}\gamma_2^{\rm OMA}}. \quad (36)$$

B. NOMA with Static PA Scheme

In the NOMA with static PA scheme, the OP of the backscatter link is expressed as

$$P_{\rm b,out}^{\rm ST} = 1 - \underbrace{\Pr\left(P_{\rm e} \geq P_{\rm c}, \gamma_{\rm r,s}^{\rm (I)} \geq \gamma_1, \gamma_{\rm r,c}^{\rm (I)} \geq \gamma_2\right)}_{P_{\rm b,1}^{\rm ST}} \times \underbrace{\Pr\left(\gamma_{\rm d,s}^{\rm ST} \geq \gamma_1, \gamma_{\rm d,c}^{\rm ST} \geq \gamma_2^{\rm NOMA}\right)}_{P_{\rm b,2}^{\rm ST}}, \tag{37}$$

where $\gamma_2^{\rm NOMA} = 2^{\frac{2R_2}{BT_0}} - 1$. Similar to the OMA scheme, it can be found that $P_{\rm b,1}^{\rm ST} = P_{\rm p,1}^{\rm OMA}$, and thus we only need to calculate $P_{\rm b,2}^{\rm ST}$. Based on $\gamma_{\rm d,s}^{\rm ST} = \frac{P_{\rm t} a_1^{\rm ST} |h_3|^2}{P_{\rm t} a_2^{\rm ST} |h_3|^2 + \sigma^2}$ and $\gamma_{\rm d,c}^{\rm ST} = \rho a_2^{\rm ST} |h_3|^2$, we have

$$\begin{aligned} P_{\rm b,2}^{\rm ST} &= \Pr\left(|h_3|^2 \geq \frac{\gamma_1}{\rho\left(a_1^{\rm ST} - a_2^{\rm ST}\gamma_1\right)}, |h_3|^2 \geq \frac{\gamma_2^{\rm NOMA}}{\rho a_2^{\rm ST}}\right) \\ &= \int_{a_{\rm ST}}^{\infty} f_{|h_3|^2}(x)\, dx = e^{-a_{\rm ST}\lambda_3}, \end{aligned} \tag{38}$$

where $a_{\rm ST} = \max\left(\frac{\gamma_1}{\rho\left(a_1^{\rm ST} - a_2^{\rm ST}\gamma_1\right)}, \frac{\gamma_2^{\rm NOMA}}{\rho a_2^{\rm ST}}\right)$.

C. NOMA with Dynamic PA Scheme

In the NOMA with dynamic PA scheme, the BD's signal can be successfully decoded by D if and only if R successfully decodes signals $s(n)$ and $c(k)$, and $|h_3|^2 \geq \frac{\gamma_1 + \gamma_2 + \gamma_1\gamma_2}{\rho}$. Therefore, the OP expression for the backscatter link can be written as

$$P_{\rm b,out}^{\rm DY} = 1 - \underbrace{\Pr\left(P_{\rm e} \geq P_{\rm c}, \gamma_{\rm r,s}^{\rm (I)} \geq \gamma_1, \gamma_{\rm r,c}^{\rm (I)} \geq \gamma_2\right)}_{P_{\rm b,1}^{\rm DY}} \times \underbrace{\Pr\left(|h_3|^2 \geq \frac{\gamma_1 + \gamma_2 + \gamma_1\gamma_2}{\rho}\right)}_{P_{\rm b,2}^{\rm DY}}, \tag{39}$$

where $P_{\rm b,1}^{\rm ST} = P_{\rm p,1}^{\rm OMA}$, and $P_{\rm b,2}^{\rm DY}$ can be calculated as

$$\begin{aligned} P_{\rm b,2}^{\rm DY} &= \Pr\left(|h_3|^2 \geq \frac{\gamma_1 + \gamma_2 + \gamma_1\gamma_2}{\rho}\right) \\ &= e^{-\lambda_3 \frac{\gamma_1 + \gamma_2 + \gamma_1\gamma_2}{\rho}}. \end{aligned} \tag{40}$$

Remark 4: By comparing (40) with (36), it is not hard to verify that $P_{\rm b,2}^{\rm OMA} > P_{\rm b,2}^{\rm DY}$. Based on this observation and both equations (39) and (35), we have $P_{\rm b,out}^{\rm OMA} < P_{\rm b,out}^{\rm DY}$. This can be explained as follows. In the relay-assisted MBC network, there exists a tradeoff between PU and BD in terms of OP during the second time slot. The NOMA with dynamic PA prioritizes safeguarding the PU's outage performance over minimizing the BD's OP in a best-effort manner, while the OMA puts the PU and BD signals on an equal footing.

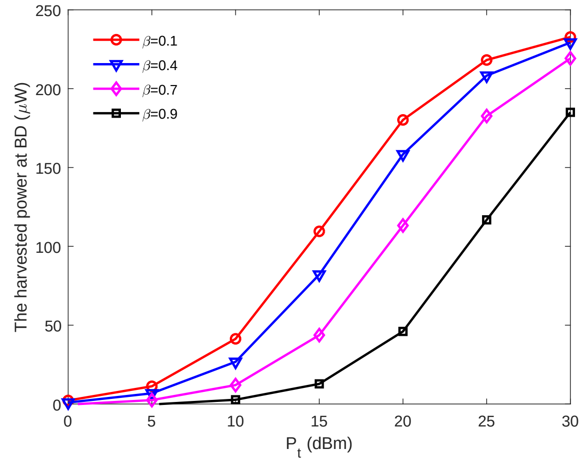

Fig. 3. The harvested power versus the transmit power.

D. Diversity Order

When $\rho \to \infty$, the backscatter link's OPs under the three forwarding schemes, i.e., $P_{\rm b,out}^{\rm OMA}$, $P_{\rm b,out}^{\rm ST}$, and $P_{\rm b,out}^{\rm DY}$, are all proportional to $1 - e^{-\frac{1}{\rho}}$. Accordingly, the diversity orders of the backscatter link under the three forwarding schemes can be computed as

$$\begin{aligned} d_{\rm b}^{\rm OMA} = d_{\rm b}^{\rm ST} = d_{\rm b}^{\rm DY} &= -\lim_{\rho\to\infty} \frac{\lg\left(P_{\rm p,out}^{\rm OMA}\right)}{\lg(\rho)} \\ &= -\lim_{\rho\to\infty} \frac{\lg\left(1 - e^{-\frac{1}{\rho}}\right)}{\lg(\rho)} = 1. \end{aligned} \tag{41}$$

V. Numerical Results

This section conducts computer simulations to assess and compare the outage performance of the proposed network with traditional decode-and-forward relay communication (referred to as "traditional relay" in the following figures) and relay-assisted PBC under energy-causality constraints. In the traditional relay, there are only three nodes, i.e., PU, R and D, where PU communicates with D through a decode-and-forward R. In the relay-assisted PBC, PU, BD, and R form a PBC in the first time slot, with the transmission following the structure of our proposed network in the second time slot. Unless otherwise specified, we adopt the following system parameters in simulations: $M = 20$, $v = 2.7$, $L = 128$, $\sigma^2 = -130\,$dBm, $\beta = 0.4$, $a_1^{\rm ST} = 0.9$, $a_2^{\rm ST} = 0.1$, $\frac{R_1}{B} = 2\,$bit/Hz, and $\frac{R_2}{B} = 0.01\,$bit/Hz, $d_0 = 100$m, $d_1 = 5$m, $d_2 = 95$m, and $d_3 = 80$m. Besides, we adopt the identical nonlinear EH model and all the parameters as detailed in [8], and its harvested power under different PRC can be found in Fig. 3.

Fig. 4 shows the OP of the primary link versus the distance d_0 between PU and R under each scheme. It can be seen that the theoretical curves of the primary link OP under the OMA scheme, static PA scheme and dynamic PA scheme based on (21), (28) and (31) match well with simulation results those are obtained by over 1×10^6 Monte Carlo simulations.

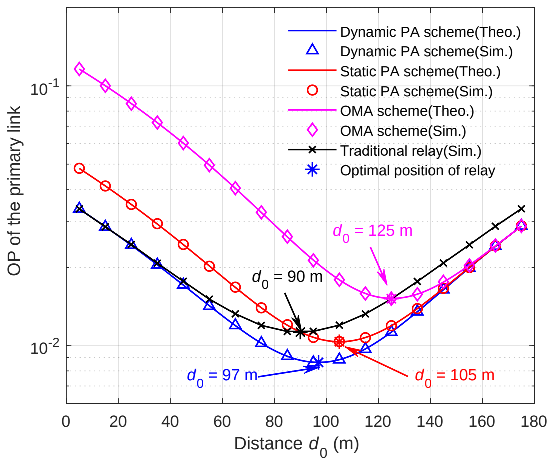

Fig. 4. OP of the primary link versus the distance d_0.

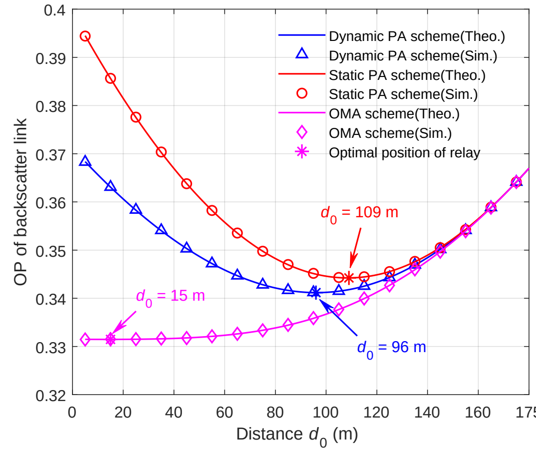

Fig. 5. OP of the backscatter link versus the PU-to-R distance d_0.

This observation demonstrates the accuracy of the derivation of the primary link OPs even at a small value of M, i.e., $M = 20$. It can also be seen that the dynamic PA scheme achieves the lowest OP while the OP under the OMA scheme is the highest, as expected in *Remark 3*. Additionally, other observations are drawn as follows: 1) Through comparison between our considered network and the traditional relay, it is found that the mutualistic relationship[9] between PU and BD in both OMA and static PA schemes is affected by distance d_0. Specifically, when R is close to PU, BD's access degrades PU's performance, indicating a lack of mutualism, i.e., the access of BD improves the PU's outage performance. Conversely, when R is distant from PU, BD's access enhances PU's outage performance, establishing mutualism between them. However, the dynamic PA scheme ensures that PU continues to benefit during BD access[10], maintaining the mutualistic relationship regardless of changes in the distance d_0. Accordingly, the OMA and the NOMA with static PA may not ensure that the access of BD improves the PU's outage performance, while it can be guaranteed by the NOMA with dynamic PA. This observation is caused by the interference control strategies employed in forwarding schemes. In the NOMA with dynamic PA scheme, the transmission of PU's signal takes precedence over that of BD's signal in the second time slot, indicating that forwarding the BD's signal will not degrade the outage performance of the PU's signal in the second time slot. However, the NOMA with static PA scheme and the OMA scheme do not ensure the priority to forward PU's signal, leading to a performance degradation in the second slot. Accordingly, the backscatter link may not improve the primary link's outage performance. 2) As d_0 increases, the OP of the primary link under each scheme shows a tendency of decreasing and then increasing, indicating that there exists an optimal R location. The optimal distances d_0 under the dynamic PA scheme, the static PA scheme, and the OMA scheme are in ascending order.

Fig. 5 shows the OPs of the backscatter link versus the distance d_0 for the three forwarding schemes. One observation is that the OPs under the OMA scheme, the static PA scheme, and the dynamic PA scheme, which are calculated by (35), (37), and (39) respectively, align perfectly with the Monte Carlo simulation results. Besides, we also observe that the OMA achieves the best outage performance, which is consistent with *Remark 4*. Another observation is that with the increase of d_0, the OPs of the backscatter link under the three schemes follow a decreasing-then-increasing trend. This indicates an optimal distance d_0 exists for each scheme. It is notable that R's location that minimizes the backscatter link's OP in the OMA scheme is very close to the PU compared to the other two schemes and the reason is summarized below. When in the OMA scheme, BD utilizes significantly more communication resources in the second time slot than in the other two schemes, while the BD's throughput is much smaller than that of PU, leading to inefficient resource utilization. Consequently, the outage performance of the backscatter link is primarily influenced by the OP of BD's signals during the first time slot. As R moves closer to the PU, the OP of BD's signals during the first time slot decreases significantly. Comparing the observation in Fig. 5 with that of Fig. 4, we find that the location of R to minimize the PU's OP is different from that to minimize the BD's OP. This suggests a tradeoff between BD's OP and PU's OP in optimizing R's location.

Fig. 6 illustrates the impact of transmit power on the OP of the primary link, considering the following five schemes, i.e., the OMA scheme, the static PA scheme, and the dynamic PA scheme in the MBC, as well as the traditional relay network and the relay-assisted PBC network with the static PA scheme. As depicted in this figure, we can see that the slope of the OP curves for the three proposed forwarding schemes approaches 1 as the transmit power increases, validating the theoretical derivation based on (34) regarding the diversity

[9]The mutualistic relationship indicates that BD shares the spectrum and energy resources with PU, while boosting the outage performance of PU. In our considered relay-assisted MBC network, BD always shares the spectrum and energy resources with PU, thus the mutualistic relationship depends on whether allowing BD to share spectrum and energy sources boosts PU's outage performance or not

[10]The detailed reasons can be found in *Remark 2*.

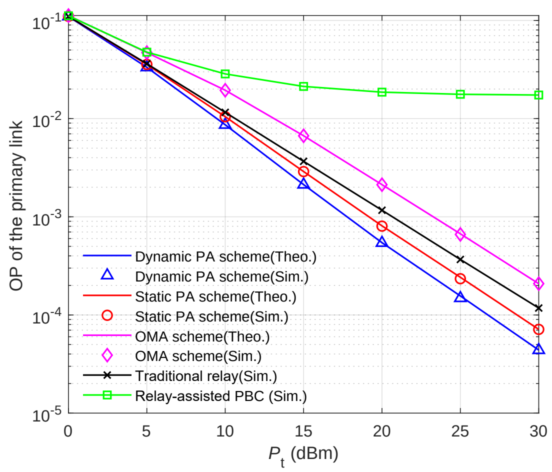

Fig. 6. OP of the primary link versus the transmit power P_t.

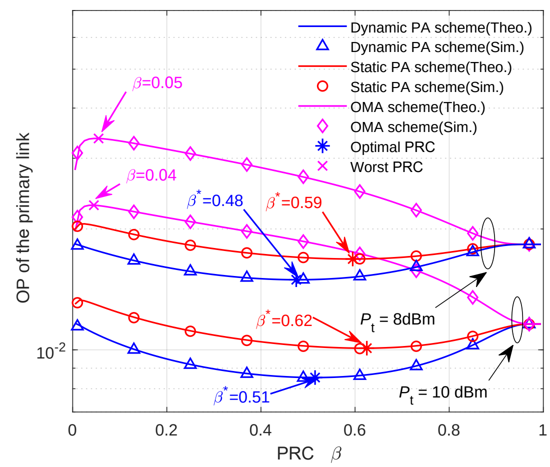

Fig. 8. OP of primary link versus β for different transmit power levels.

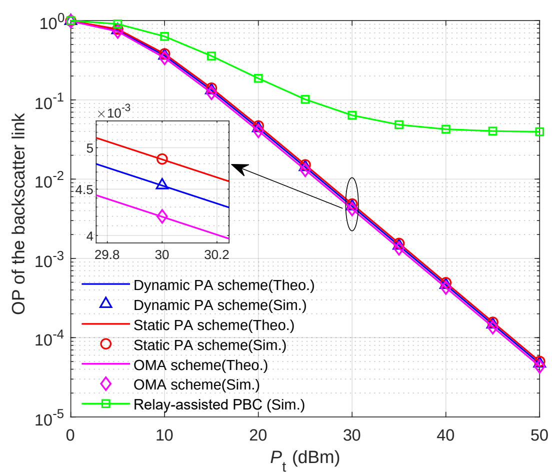

Fig. 7. OP of backscatter link versus the transmit power P_t.

gain of the primary link. In the relay-assisted PBC, when the transmit power is sufficiently large, the OP of the primary link saturates, i.e., the diversity gain is 0. This suggests that the outage performance of the primary link in the our considered network is better than that of the relay-assisted PBC network. According to Fig. 4, BD and PU establish a mutualistic relationship under the static PA scheme when $d_0 > 90$ m. Therefore, the outage performance of the primary link under both the dynamic PA scheme and the static PA scheme is superior to that of traditional relay network as BD's access can enhance PU performance.

Fig. 7 plots the backscatter link's OP as a function of transmit power under the three proposed forwarding schemes and the relay-assisted PBC network with the static PA scheme. It can be seen that the diversity order of the backscatter links for the OMA scheme, the static PA scheme, and the dynamic PA scheme in the MBC equals indeed one, which validates our theoretical analysis, while in the relay-assisted PBC, there is an error floor that leads to zero diversity order. This confirms the advantage of our considered network over the relay-assisted PBC network.

Fig. 8 illustrates the OPs for the primary link versus the PRC of BD at different transmit powers, i.e., $P_{\rm t} = 8\,{\rm dBm}$ and $P_{\rm t} = 10\,{\rm dBm}$. We can see that when R adopts the OMA forwarding scheme, the OP of the primary link shows a trend of increasing and then decreasing with the PRC of the BD, which indicates that there is a PRC that leads to the worst outage performance of the primary link. The reason for this phenomenon is that under this network parameter setting, with a small value of β, the access of BD enhances the PU's throughput in the first phase but BD's signal is highly unlikely to be decoded by R. This allows R only forwarding's PU's signal and thus the PU's outage performance is enhanced. However, when β exceeds a certain vale, the probability that BD's signal is decoded at R increases, and in this case, R should allocate resource to forward BD's signal and this will degrade the PU's outage performance. Another observation is that with the increase of β, the OPs of the static PA scheme and the dynamic PA scheme show a tendency of decreasing and then increasing, thus the PRCs that make the best performance of the primary link outage performance exist in each of these two forwarding schemes. Additionally, the optimal PRC of the dynamic PA scheme is smaller than that of the static PA scheme. The reasons are summarized below. Since the energy-causality constraint is considered at BD, a large β leads to a high probability that BD is inactivated. This may contribute to the PU's outage performance of the static PA scheme where if the BD's signal is forwarded by R, the PU's outage performance degrades. However, this will not happen in the dynamic PA scheme since it strictly keeping PU's OP same as the scenario with only PUs signal being forwarded by R. Due to the above reasons, the optimal PRC under the dynamic PA scheme is smaller than that of the static PA scheme.

Fig. 9 displays the OPs for the backscatter link as a function of BD's PRC at $P_{\rm t} = 8\,{\rm dBm}$ and $P_{\rm t} = 10\,{\rm dBm}$, respectively. It can be seen the OP of the backscatter link in all three forwarding schemes decreases and then increases with the PRC of BD. That is to say, there exists an optimal PRC

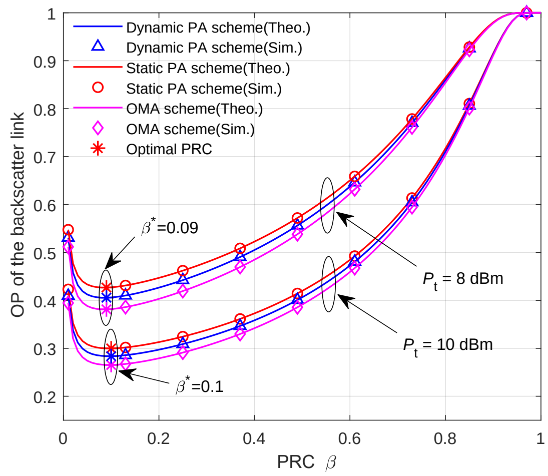

Fig. 9. OP of backscatter link versus β for different transmit power levels.

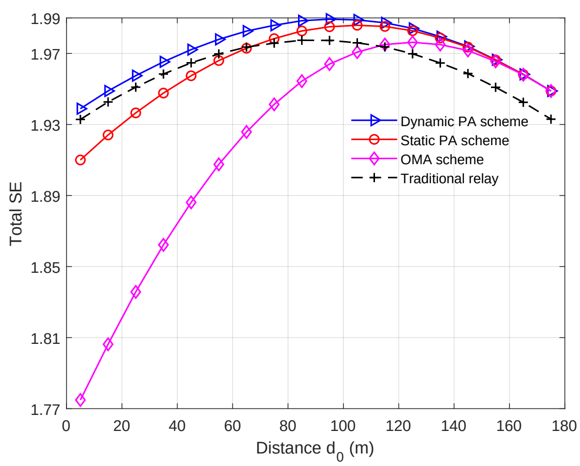

Fig. 10. Total SE versus the PU-to-R distance d_0.

that maximizes the performance of the backscatter link. It can also be seen that if for minimizing BD's OP, the optimal β should increase with the transmit power. Comparing the result in Fig. 9 with that of Fig. 8, we confirm that the optimal β to minimize the PU's OP differs from that to minimize the BD's OP. This suggests a tradeoff between BD's OP and PU's OP in optimizing β.

Finally, we evaluate the total spectrum efficiency (SE) of both primary and backscatter links in Fig. 10. The total SE is calculated as $\frac{R_1}{B}\left(1 - \text{OP of the primary link}\right) + \frac{R_2}{B}\big(1 - \text{OP of the backscatter link}\big)$. One observation is that the NOMA with dynamic PA scheme achieves the highest SE among these schemes. This is because the NOMA with dynamic PA yields the lowest primary link's OP among these schemes, as verified in Fig. 4. Although the backscatter link's OP of the NOMA with dynamic PA is not the lowest, as shown in Fig. 5, the required BD's throughput is much smaller than that of PU. Another observation is that an optimal R location exists to maximize the total SE and the optimal R location for maximizing the total SE almost equals that for minimizing the OP of the primary link.

VI. Conclusion

In this paper, we have proposed and investigated a relay-assisted MBC network in terms of OP under energy-causality constraint and three proposed forwarding strategies. The closed-form OP expressions under three schemes for the primary and backscatter links and their diversity orders have been derived. Computer simulations have verified our theoretical analysis. We have also obtained insights into the relay-assisted BC network. First, in the relay-assisted MBC, the backscatter link may not enhance the PU's outage performance, which is different from the traditional MBC with existing direct links between PU/BD and D. Second, in the proposed three forwarding strategies, only the NOMA with dynamic PA can ensure that the access of BD enhances the PU's outage performance. Third, the optimal values of the BD's PRC and R's location that minimize the PU's OP are different from those that minimize the BD's OP. This indicates that the setting of BD's PRC and R's location in relay-assisted MBC requires the consideration of the tradeoff between BD's OP and PU's OP.

Appendix A

To successfully decode $\widehat{s}(i)$ and $\widehat{c}(i)$ at D, the following two inequalities should be satisfied, i.e.,

$$R_{\rm d,s}^{\rm DY} \geq R_1, \tag{A.1}$$

$$R_{\rm d,c}^{\rm DY} \geq R_2. \tag{A.2}$$

By substituting $\gamma_{\rm d,s}^{\rm DY} = \frac{P_{\rm t} a_1^{\rm DY}|h_3|^2}{P_{\rm t} a_2^{\rm DY}|h_3|^2+\sigma^2}$ and $a_2^{\rm DY} = 1 - a_1^{\rm DY}$ into (A.1) and performing simple mathematical operations, it can be concluded that to ensure the success of decoding $\widehat{s}(i)$, $a_1^{\rm DY}$ should meet

$$a_1^{\rm DY} \geq \frac{P_{\rm t}\gamma_1|h_3|^2 + \gamma_1\sigma^2}{P_{\rm t}|h_3|^2 + P_{\rm t}\gamma_1|h_3|^2}, \tag{A.3}$$

where $\gamma_1 = 2^{\frac{2R_1}{BT_0}} - 1$.

Similarly, by substituting $\gamma_{\rm d,c}^{\rm DY} = \rho a_2^{\rm DY}|h_3|^2$ and $a_2^{\rm DY} = 1 - a_1^{\rm DY}$ into (A.2), for successfully decoding $\widehat{c}(i)$, $a_1^{\rm DY}$ should satisfy

$$a_1^{\rm DY} \leq 1 - \frac{\gamma_2\sigma^2}{P_{\rm t}|h_3|^2}, \tag{A.4}$$

where $\gamma_2 = 2^{\frac{2LR_2}{BT_0}} - 1$.

Based on (A.3) and (A.4), we conclude that if $\frac{P_{\rm t}\gamma_1|h_3|^2+\gamma_1\sigma^2}{P_{\rm t}|h_3|^2+P_{\rm t}\gamma_1|h_3|^2} \leq a_1^{\rm DY} \leq 1 - \frac{\gamma_2\sigma^2}{P_{\rm t}|h_3|^2}$ holds, both $\widehat{s}(i)$ and $\widehat{c}(i)$ can be successfully decoded by D. To ensure $\frac{P_{\rm t}\gamma_1|h_3|^2+\gamma_1\sigma^2}{P_{\rm t}|h_3|^2+P_{\rm t}\gamma_1|h_3|^2} \leq 1 - \frac{\gamma_2\sigma^2}{P_{\rm t}|h_3|^2}$, $|h_3|^2 \geq \frac{\gamma_1+\gamma_2+\gamma_1\gamma_2}{\rho}$ should be satisfied. Therefore, in the case of $|h_3|^2 \geq \frac{\gamma_1+\gamma_2+\gamma_1\gamma_2}{\rho}$, if $a_1^{\rm DY}$ takes any value in the interval $\left[\frac{P_{\rm t}\gamma_1|h_3|^2+\gamma_1\sigma^2}{P_{\rm t}|h_3|^2+P_{\rm t}\gamma_1|h_3|^2}, 1 - \frac{\gamma_2\sigma^2}{P_{\rm t}|h_3|^2}\right]$, D can successfully decode both $\widehat{s}(i)$ and $\widehat{c}(i)$. In the case of $|h_3|^2 < \frac{\gamma_1+\gamma_2+\gamma_1\gamma_2}{\rho}$, it is not hard to verify $\frac{P_{\rm t}\gamma_1|h_3|^2+\gamma_1\sigma^2}{P_{\rm t}|h_3|^2+P_{\rm t}\gamma_1|h_3|^2} >$

$1-\frac{\gamma_2\sigma^2}{P_{\rm t}|h_3|^2}$. This means both (A.3) and (A.4) cannot be met at the same time. Combined with the adopted SIC order at D, only the PU's signal is forwarded, leading to an outage event of the BD's transmission. In this case, to minimize the PU's OP, the optimal $a_1^{\rm DY}$ and $a_2^{\rm DY}$ should be set as 1 and 0, respectively. The proof is complete.

Appendix B

According to the value range of $|h_0|^2$, $P_{\rm p,1}^{\rm OMA}$ can be calculated as

$$\begin{aligned} P_{\rm p,1}^{\rm OMA} &= \Pr\begin{pmatrix} |h_1|^2 \geq b_1, \rho\beta L|h_1|^2|h_2|^2 \geq \gamma_2, \\ \rho\left(|h_0|^2+\beta|h_1|^2|h_2|^2\right) \geq \gamma_1 \end{pmatrix} \\ &\overset{(a)}{=} \underbrace{\Pr\left(|h_1|^2 \geq \max\left(b_1, \frac{b_2-|h_0|^2}{\beta|h_2|^2}\right), |h_0|^2 < b_4\right)}_{Q_1} \\ &+ \underbrace{\Pr\left(|h_1|^2 \geq \max\left(b_1, \frac{b_3}{|h_2|^2}\right), |h_0|^2 \geq b_4\right)}_{Q_2}, \end{aligned} \tag{B.1}$$

where $b_1=\frac{\phi}{(1-\beta)P_{\rm t}}$, $b_2=\gamma_1\rho^{-1}$, $b_3=\frac{\gamma_2}{\rho\beta L}$, $b_4=b_2-\beta b_3$, and step (a) is derived from the total probability formula, i.e., $\frac{b_2-|h_0|^2}{\beta|h_2|^2}>\frac{b_3}{|h_2|^2}$ and $\frac{b_2-|h_0|^2}{\beta|h_2|^2}\leq\frac{b_3}{|h_2|^2}$.

To remove the max function in Q_1,we have

$$\begin{aligned} Q_1 &= \underbrace{\Pr\left(|h_1|^2 \geq \frac{b_2-|h_0|^2}{\beta|h_2|^2}, b_1 \leq \frac{b_2-|h_0|^2}{\beta|h_2|^2}, |h_0|^2 < b_4\right)}_{Q_{11}} \\ &+ \underbrace{\Pr\left(|h_1|^2 \geq b_1, |h_0|^2 \geq b_2 - b_1\beta|h_2|^2, |h_0|^2 < b_4\right)}_{Q_{12}}. \end{aligned} \tag{B.2}$$

After some manipulations, Q_{11} can be calculated as

$$Q_{11} = \underbrace{b_5\int_{b_1}^{\infty}\frac{z}{\beta\lambda_0 z-\lambda_2}e^{-\lambda_1 z}f(z)\,{\rm d}z}_{Q_{111}} - \underbrace{b_6 {\rm b}_7 e^{-\lambda_1 b_1}}_{Q_{112}}, \tag{B.3}$$

where $b_5=\beta\lambda_1\lambda_0 e^{-\lambda_0 b_2}$, $f(z)=e^{\left(\lambda_0-\frac{\lambda_2}{\beta z}\right)b_2}-e^{\left(\lambda_0-\frac{\lambda_2}{\beta z}\right)\frac{\gamma_2}{\rho L}}$, $b_6=\frac{\beta\phi\lambda_0}{\beta\phi\lambda_0-\lambda_2(1-\beta)P}$, $b_7=e^{-\frac{\lambda_2 b_2}{b_1\beta}}-e^{\left(\lambda_0-\frac{\lambda_2}{b_1\beta}\right)\frac{\gamma_2}{\rho L}-\lambda_0 b_2}$.

Clearly, Q_{111} is non-integrable because of $e^{-\lambda_1 z}f(z)$ involved in the integrand. Thus, we use Gauss-Chebyshev quadrature[11] [37] to approximate Q_{111}. Particularly, letting $z=\tan\theta,\theta\in\left(\arctan b_1,\frac{\pi}{2}\right)$ and using Gauss-Chebyshev quadrature approximation, Q_{111} is approximated as

$$\begin{aligned} Q_{111} &\approx \frac{1}{4}\beta\lambda_1\lambda_0 e^{-\lambda_0 b_2}\left(\pi-2\arctan b_1\right) \\ &\times \sum_{m=1}^{M} w\sqrt{1-c_m^2}\frac{\tan\theta_m {\rm sec}^2\theta_m e^{-\lambda_1\tan\theta_m}}{\beta\lambda_0\tan\theta_m-\lambda_2} \\ &\times \left(e^{\left(\lambda_0-\frac{\lambda_2}{\beta\tan\theta_m}\right)b_2}-e^{\left(\lambda_0-\frac{\lambda_2}{\beta\tan\theta_m}\right)\frac{\gamma_2}{\rho L}}\right), \end{aligned} \tag{B.4}$$

where $\theta_m=\frac{\pi-2\arctan b_1}{4}\cos\left(\frac{2m-1}{2M}\pi\right)+\frac{\pi+2\arctan b_1}{4}$, $c_m=\cos\left(\frac{2m-1}{2M}\pi\right)$, $w=\frac{\pi}{M}$, and M is a complexity-accuracy tradeoff parameter.

Then we derive Q_{12} into the closed form. Due to $b_2-|h_0|^2>b_3\ \beta>0$, we rewrite Q_{12} as

$$\begin{aligned} Q_{12} &= \Pr\left(|h_1|^2 \geq b_1, |h_2|^2 \geq \left(b_2-|h_0|^2\right)\big/ b_1\beta, |h_0|^2 < b_4\right) \\ &= \int_{b_1}^{\infty}\int_{0}^{b_4}\int_{\frac{(b_2-y)}{b_1\beta}}^{\infty} f_{|h_2|^2}(x) f_{|h_0|^2}(y) f_{|h_1|^2}(z)\,{\rm d}x{\rm d}y{\rm d}z \\ &= b_6 e^{-\lambda_1 b_1-\frac{\lambda_2 b_2}{b_1\beta}}\left(1-e^{b_4\left(\frac{\lambda_2}{b_1\beta}-\lambda_0\right)}\right). \end{aligned} \tag{B.5}$$

Similarly, Q_2 can be rewritten as

$$\begin{aligned} Q_2 &= \underbrace{\Pr\left(|h_1|^2 \geq \frac{b_3}{|h_2|^2}, \frac{b_3}{|h_2|^2} \geq b_1, |h_0|^2 \geq b_4\right)}_{Q_{21}} \\ &+ \underbrace{\Pr\left(|h_1|^2 \geq b_1, \frac{b_3}{|h_2|^2} < b_1, |h_0|^2 \geq b_4\right)}_{Q_{22}} \\ &= \underbrace{\lambda_2 {\rm e}^{-\lambda_0 b_4}\int_{0}^{\frac{b_3}{b_1}} e^{-\lambda_2 y-\frac{\lambda_1 b_3}{y}}dy}_{Q_{21}} + \underbrace{e^{\left(-\lambda_1 b_1-\frac{\lambda_2 b_3}{b_1}-\lambda_0 b_4\right)}}_{Q_{22}}. \end{aligned} \tag{B.6}$$

Using Gauss-Chebyshev quadrature to approximate Q_{21}, we have

$$Q_{21} \approx \frac{\lambda_2 b_3}{2b_1}e^{-\lambda_0 b_4}\sum_{m=1}^{M} w\sqrt{1-c_m^2}e^{-\lambda_2 d_m-\frac{\lambda_1 b_3}{d_m}}, \tag{B.7}$$

where $d_m=\frac{b_3(c_m+1)}{2b_1}$.

Until now, $P_{\rm p,1}^{\rm OMA}$ has been derived and the proof is complete.

[11]For a highly complex integral, there are generally two ways to find a closed-form expression. One is to use boundaries to compute integrals by means of inequalities. The other is based on approximations such as the Gauss-Chebyshev quadrature. Herein, Gauss-Chebyshev quadrature is adopted because it can provide sufficient accuracy in very few terms. Please note that Gauss-Chebyshev quadrature has been widely used in evaluating transmission performance of a wireless communication network (see [8], [25], [26], [36] for example).

Appendix C

$P_{\mathrm{p},3}^{\mathrm{OMA}}$ can be expressed as

$$\begin{aligned}
P_{\mathrm{p},3}^{\mathrm{OMA}} &= \Pr\left(\begin{array}{l} |h_1|^2 \geq b_1, |h_1|^2|h_2|^2 < b_3, \\ |h_0|^2 + \beta|h_1|^2|h_2|^2 \geq b_2 \end{array} \right) \\
&= \Pr\left(|h_1|^2 \geq b_1, |h_1|^2 < \frac{b_3}{|h_2|^2}, |h_1|^2 \geq \frac{X}{\beta|h_2|^2} \right) \\
&= \underbrace{\Pr\left(\frac{X}{\beta|h_2|^2} \leq |h_1|^2 < \frac{b_3}{|h_2|^2}, |h_2|^2 < \frac{X}{\beta b_1}, X < \beta b_3 \right)}_{Q_3} \\
&\quad \underbrace{+ \Pr\left(b_1 \leq |h_1|^2 < \frac{b_3}{|h_2|^2}, X \leq \beta b_1 |h_2|^2, |h_2|^2 < \frac{b_3}{b_1} \right)}_{Q_4}, \quad \text{(C.1)}
\end{aligned}$$

where $X = b_2 - |h_0|^2$ and its probability density function can be expressed as $f_X(x) = \begin{cases} \lambda_0 e^{-\lambda_0(b_2-x)} & , x \leq b_2 \\ 0 & , x > b_2 \end{cases}$.

Q_3 is equivalent to

$$\begin{aligned}
Q_3 &= \int_{-\infty}^{\beta b_3} \int_0^{\frac{X}{\beta b_1}} \int_{\frac{x}{\beta y}}^{\frac{b_3}{y}} f_{|h_1|^2}(z) f_{|h_2|^2}(y) f_X(x)\, dz dy dx \\
&= \underbrace{\int_0^{\beta b_3} \int_0^{\frac{X}{\beta b_1}} \lambda_2 e^{-\lambda_2 y - \lambda_1 \frac{x}{\beta y}} f_X(x)\, dy dx}_{Q_{31}} \\
&\quad \underbrace{- \int_0^{\beta b_3} \int_0^{\frac{X}{\beta b_1}} \lambda_2 e^{-\lambda_2 y - \lambda_1 \frac{b_3}{y}} f_X(x)\, dy dx}_{Q_{32}}. \quad \text{(C.2)}
\end{aligned}$$

Using Gauss-Chebyshev quadrature and [38, eq. (2.321.2)], we calculate Q_{31} as

$$\begin{aligned}
Q_{31} &\approx \frac{\lambda_0 \lambda_2}{2\beta b_1} e^{-\lambda_0 b_2} \sum_{m=1}^{M} w\sqrt{1-c_m^2} \\
&\quad \times e^{-\lambda_1 \frac{2b_1}{(c_m+1)}} \left(e^{\beta b_3 g_m} \left(\frac{\beta b_3}{g_m} - \frac{1}{g_m^2} \right) + \frac{1}{g_m^2} \right), \quad \text{(C.3)}
\end{aligned}$$

where $g_m = \lambda_0 - \frac{\lambda_2(c_m+1)}{2\beta b_1}$.

Q_{32} is solved in two steps. Specifically, step (a) involves swapping the order of integration, while step (b) uses Gauss-Chebyshev quadrature approximation. By doing so, we have

$$\begin{aligned}
Q_{32} &\overset{(a)}{=} \lambda_0 \lambda_2 \int_0^{\frac{b_3}{b_1}} \int_{\beta b_1 y}^{\beta b_3} e^{-\lambda_2 y - \lambda_1 \frac{b_3}{y}} e^{-\lambda_0(b_2-x)} dx dy \\
&= \lambda_2 e^{-\lambda_0 b_2} \int_0^{\frac{b_3}{b_1}} e^{-\lambda_2 y - \lambda_1 \frac{b_3}{y}} \left(e^{\beta\lambda_0 b_3} - e^{\beta\lambda_0 b_1 y} \right) dy \\
&\overset{(b)}{\approx} \frac{\lambda_2 b_3 e^{-\lambda_0 b_2}}{2b_1} \sum_{m=1}^{M} w\sqrt{1-c_m^2} \\
&\quad \times e^{-\lambda_2 u_m - \lambda_1 \frac{b_3}{u_m}} \left(e^{\beta\lambda_0 b_3} - e^{\beta\lambda_0 b_1 u_m} \right), \quad \text{(C.4)}
\end{aligned}$$

where $u_m = \frac{b_3(c_m+1)}{2b_1}$.

Next, we derive Q_4 into a closed form.

$$\begin{aligned}
Q_4 &= \int_0^{\frac{b_3}{b_1}} \int_{b_1}^{\frac{b_3}{z}} \int_{-\infty}^{\beta b_1 z} f_X(x) f_{|h_1|^2}(y) f_{|h_2|^2}(z)\, dx dy dz \\
&= \underbrace{\lambda_2 e^{-\lambda_0 b_2} \frac{e^{-\lambda_1 b_1}}{\lambda_0 \beta b_1 - \lambda_2} \left(e^{(\lambda_0 \beta b_1 - \lambda_2)\frac{b_3}{b_1}} - 1 \right)}_{Q_{41}} \\
&\quad \underbrace{- \lambda_2 e^{-\lambda_0 b_2} \int_0^{\frac{b_3}{b_1}} e^{\lambda_0 \beta b_1 z - \lambda_2 z - \lambda_1 \frac{b_3}{z}} dz}_{Q_{42}}. \quad \text{(C.5)}
\end{aligned}$$

Using Gauss-Chebyshev quadrature, we can approximate Q_{42} as

$$Q_{42} \approx \frac{\lambda_2 b_3 e^{-\lambda_0 b_2}}{2b_1} \sum_{m=1}^{M} w\sqrt{1-c_m^2} e^{\lambda_0 \beta b_1 r_m - \lambda_2 r_m - \lambda_1 \frac{b_3}{r_m}}, \quad \text{(C.6)}$$

where $r_m = \frac{b_3(c_m+1)}{2b_1}$.

Substituting (C.3), (C.4), and (C.5) into (C.1), the expression of $P_{\mathrm{p},3}^{\mathrm{OMA}}$ can be obtained, and the proof is complete.

References

[1] M. M. Butt, N. R. Mangalvedhe, N. K. Pratas, J. Harrebek, J. Kimionis, M. Tayyab, O.-E. Barbu, R. Ratasuk, and B. Vejlgaard, "Ambient IoT: A missing link in 3GPP IoT devices landscape," *IEEE Internet Things Mag.*, vol. 7, no. 2, pp. 85–92, 2024.

[2] J. Yu, C. Du, J. Liu, R. Zhang, and S. Wang, "Subscatter: Subcarrier-level ofdm backscatter," in *Proc. IEEE INFOCOM*, 2023, pp. 1–10.

[3] X. Jiang, M. Sheng, N. Zhao, J. Liu, D. Niyato, and F. R. Yu, "Outage analysis of uav-aided networks with underlaid ambient backscatter communications," *IEEE Trans. Wireless Commun.*, vol. 22, no. 11, pp. 7492–7505, 2023.

[4] B. Gu, D. Li, H. Ding, G. Wang, and C. Tellambura, "Breaking the interference and fading gridlock in backscatter communications: State-of-the-art, design challenges, and future directions," *IEEE Commun. Surveys Tut.*, pp. 1–1, 2024.

[5] J. Liu, J. Yu, X. Chen, R. Zhang, S. Wang, and J. An, "Covert communication in ambient backscatter systems with uncontrollable RF source," *IEEE Trans. Commun.*, vol. 70, no. 3, pp. 1971–1983, 2022.

[6] Y.-C. Liang, Q. Zhang, E. G. Larsson, and G. Y. Li, "Symbiotic radio: Cognitive backscattering communications for future wireless networks," *IEEE Trans. Cognit. Commun. Netw.*, vol. 6, no. 4, pp. 1242–1255, 2020.

[7] R. Long, Y. C. Liang, H. Guo, G. Yang, and R. Zhang, "Symbiotic radio: A new communication paradigm for passive internet of things," *IEEE Internet Things J.*, vol. 7, no. 2, pp. 1350–1363, 2020.

[8] Y. Ye, L. Shi, X. Chu, and G. Lu, "On the outage performance of ambient backscatter communications," *IEEE Internet Things J.*, vol. 7, no. 8, pp. 7265–7278, 2020.

[9] M. Elsayed, A. Samir, A. A. A. El-Banna, X. Li, and B. M. ElHalawany, "When NOMA multiplexing meets symbiotic ambient backscatter communication: Outage analysis," *IEEE Trans. Veh. Technol.*, vol. 71, no. 1, pp. 1026–1031, 2022.

[10] H. Yang, H. Ding, and M. Elkashlan, "Opportunistic symbiotic backscatter communication systems," *IEEE Commun. Lett.*, vol. 27, no. 1, pp. 100–104, 2023.

[11] Y. Ye, R. Xu, G. Chen, D. B. da Costa, and G. Lu, "QoS-guaranteed adaptive power reflection coefficient for self-powered cooperative ambient backscatter communication," *IEEE Wireless Commun. Lett.*, pp. 1–1, 2024.

[12] H. Ding, M.-S. Alouini, K. Xin, H. Li, and S. Xu, "Symbiotic ambient backscatter systems: Outage behavior and ergodic capacity," *IEEE Internet Things J.*, vol. 9, no. 23, pp. 23 670–23 690, 2022.

[13] X. Kang, Y.-C. Liang, and J. Yang, "Riding on the primary: A new spectrum sharing paradigm for wireless-powered iot devices," *IEEE Trans. Wireless Commun.*, vol. 17, no. 9, pp. 6335–6347, 2018.

[14] R. Long, G. Yang, Y. Pei, and R. Zhang, "Transmit beamforming for cooperative ambient backscatter communication systems," in *Proc. IEEE GLOBECOM*, 2017, pp. 1–6.

[15] H. Yang, H. Ding, K. Cao, M. Elkashlan, H. Li, and K. Xin, "A ris-segmented symbiotic ambient backscatter communication system," *IEEE Trans. Veh. Technol.*, vol. 73, no. 1, pp. 812–825, 2024.

[16] H. Yang, H. Ding, M. Elkashlan, H. Li, and K. Xin, "A novel symbiotic backscatter-NOMA system," *IEEE Trans. Veh. Technol.*, vol. 72, no. 8, pp. 11 006–11 011, 2023.

[17] J. Liu, H. Ding, M. Elkashlan, W. Chen, S. Wang, and T. Sun, "A STAR-RIS-segmented symbiotic AmBC system," *IEEE Wireless Commun. Lett.*, vol. 13, no. 5, pp. 1379–1383, 2024.

[18] Z. Wen, H. Ding, M. Elkashlan, C. Yuen, J. M. Moualeu, J. Liu, K. Xin, and C. Yang, "Outage analysis for a STAR-RIS-segmented symbiotic backscatter NOMA system," *IEEE Trans. Commun.*, pp. 1–1, 2024.

[19] H. Yang, Y. Ye, K. Liang *et al.*, "Energy efficiency maximization for symbiotic radio networks with multiple backscatter devices," *IEEE Open J. Commun. Soc.*, vol. 2, pp. 1431–1444, 2021.

[20] S. Zhou, W. Xu, K. Wang, C. Pan, M. S. Alouini *et al.*, "Ergodic rate analysis of cooperative ambient backscatter communication," *IEEE Wireless Commun. Lett.*, vol. 8, no. 6, pp. 1679–1682, 2019.

[21] Q. Zhang, Y. C. Liang, H. C. Yang, and H. V. Poor, "Mutualistic mechanism in symbiotic radios: When can the primary and secondary transmissions be mutually beneficial?" *IEEE Trans. Wireless Commun.*, vol. 21, no. 10, pp. 8036–8050, 2022.

[22] Y. Ye, L. Shi, X. Chu, G. Lu, and S. Sun, "Mutualistic cooperative ambient backscatter communications under hardware impairments," *IEEE Trans. Commun.*, vol. 70, no. 11, pp. 7656–7668, 2022.

[23] Y. Ye *et al.*, "Impacts of hardware impairments on mutualistic cooperative ambient backscatter communications," in *Proc. IEEE ICC*, 2022, pp. 5372–5377.

[24] Y. Guo, G. Wang, R. Xu, R. He, X. Wei, and C. Tellambura, "Capacity analysis for wireless symbiotic communication systems with BPSK tags under sensitivity constraint," *IEEE Commun. Lett.*, vol. 26, no. 1, pp. 44–48, 2022.

[25] W. Zhao, J. Zhu, X. She, G. Wang, and C. Tellambura, "Ergodic capacity analysis for cooperative ambient communication system under sensitivity constraint," *IEEE Commun. Lett.*, vol. 27, no. 10, pp. 2822–2826, 2023.

[26] J. Wang, X. Ding, Q. Zhang, and Y.-C. Liang, "Multiple access design for symbiotic radios: Facilitating massive IoT connections with cellular networks," *IEEE Trans. Wireless Commun.*, vol. 23, no. 1, pp. 201–216, 2024.

[27] D. V. Rodrigues, D. Rodriguez, J. Wang, and C. Li, "Smaller and with more bars: A relay transceiver for IoT/5G applications," *IEEE Microw. Mag.*, vol. 21, no. 1, pp. 96–100, 2020.

[28] R. Xu, Y. Ye, H. Sun *et al.*, "Wireless powered opportunistic cooperative backscatter communications: To relay or not?" in *Proc. IEEE VTC-Spring*, Helsinki, Finland, 2022, pp. 1–5.

[29] S. Gong, Y. Zou, D. T. Hoang, J. Xu *et al.*, "Capitalizing backscatter-aided hybrid relay communications with wireless energy harvesting," *IEEE Internet Things J.*, vol. 7, no. 9, pp. 8709–8721, 2020.

[30] Z. Niu, W. Ma, W. Wang, and T. Jiang, "Spatial modulation-based ambient backscatter: Bringing energy self-sustainability to massive internet of everything in 6G," *China Commun.*, vol. 17, no. 12, pp. 52–65, 2020.

[31] Z. Niu, L. Xiao, J. Kan, S. He, and T. Jiang, "A unified implementation framework for index modulation assisted MIMO backscatter communication," *IEEE Communications Letters*, vol. 27, no. 5, pp. 1422–1426, 2023.

[32] H. Ding, X. Wang, D. B. da Costa, Y. Chen, and F. Gong, "Adaptive time-switching based energy harvesting relaying protocols," *IEEE Trans. Commun.*, vol. 65, no. 7, pp. 2821–2837, 2017.

[33] P. Chen, H. Liu, Y. Ye, L. Yang, K. J. Kim, and T. A. Tsiftsis, "Rate-splitting multiple access aided mobile edge computing with randomly deployed users," *IEEE J. Sel. Areas Commun.*, vol. 41, no. 5, pp. 1549–1565, 2023.

[34] L. Lv, D. Xu, R. Q. Hu, Y. Ye, L. Yang, X. Lei, X. Wang, D. I. Kim, and A. Nallanathan, "Safeguarding next generation multiple access using physical layer security techniques: A tutorial," 2024.

[35] R. Narasimhan, "Finite-SNR diversity-multiplexing tradeoff for correlated rayleigh and rician MIMO channels," *IEEE Trans. Inf. Theory*, vol. 52, no. 9, pp. 3965–3979, 2006.

[36] Z. Liu, G. Lu, Y. Ye, and X. Chu, "System outage probability of PS-SWIPT enabled two-way AF relaying with hardware impairments," *IEEE Trans. Veh. Technol.*, vol. 69, no. 11, pp. 13 532–13 545, 2020.

[37] E. Hildebrand and I. M. Ryzhik, *Introduction to numerical analysis*. New York, USA: Dover, 1987.

[38] I. S. Gradshteyn and I. M. Ryzhik, *Table of Integrals, Series, and Products*. New York, NY, USA: Academic, 2007.

Yinghui Ye received the Ph.D. degree in communication and information system from Xidian Univeristy in 2020. Since 2020, he joined the Department of Communication and Information Engineering in Xi'an University of Posts and Telecommunications, where he is currently an Associate Professor. His research interests include mobile edge computing, wireless energy harvesting, and backscatter communications. He has authored/co-authored more than 80 technical articles in the IEEE TRANSACTIONS, JOURNALS, LETTERS AND CONFERENCES. He received the Exemplary Reviewer Award from the IEEE WIRELESS COMMUNICATIONS LETTERS in 2019. He currently serves as the Editor of PHYSICAL COMMUNICATION (ELSEVIER), and was a Guest Editor of IEEE INTERNET OF THINGS JOURNAL.

Yujia Tian received the M.S. degree from the Xi'an University of Posts and Telecommunications in 2024. He is currently working with the Shangqiu Branch of China Mobile Communications Corporation. His current research interest is backscatter communication.

Xiaoli Chu is a Professor in the Department of Electronic and Electrical Engineering at the University of Sheffield, UK. She received the B.Eng. degree in Electronic and Information Engineering from Xi'an Jiao Tong University in 2001 and the Ph.D. degree in Electrical and Electronic Engineering from the Hong Kong University of Science and Technology in 2005. From 2005 to 2012, she was with the Centre for Telecommunications Research at King's College London. Xiaoli has co-authored over 200 peer-reviewed journal and conference papers. She is co-recipient of the IEEE Communications Society 2017 Young Author Best Paper Award. She co-authored/co-edited the books "Fog-Enabled Intelligent IoT Systems"(Springer 2020), "Ultra Dense Networks for 5G and Beyond"(Wiley 2019), "Heterogeneous Cellular Networks - Theory, Simulation and Deployment"(Cambridge University Press 2013), and "4G Femtocells: Resource Allocation and Interference Management"(Springer 2013). She is Senior Editor for the IEEE WIRELESS COMMUNICATIONS LETTERS, and received the IEEE COMMUNICATIONS LETTERS Exemplary Editor Award in 2018. She was Co-Chair of Wireless Communications Symposium for IEEE ICC 2015, Workshop Co-Chair for IEEE GreenCom 2013, and has co-organized 8 workshops at IEEE ICC, GLOBECOM, WCNC, and PIMRC.

Sumei Sun (Fellow, IEEE) is a Principal Scientist, Deputy Executive Director (Research), and Head of the Communications and Networks Dept at the Institute for Infocomm Research, Singapore. She is also holding a joint appointment with the Singapore Institute of Technology, and an adjunct appointment with the National University of Singapore, both as a full professor. Her current research interests are in next-generation wireless communications, joint sensing-communication-computing-control design, and industrial internet of things. . She has been Member-at-Large of the IEEE Communications Society and is a member of the IEEE Vehicular Technology Society Board of Governors (2022-2024), Fellow of the IEEE and the Academy of Engineering Singapore.

Guangyue Lu received the Ph.D. degree from Xidian University, Xi'an, China, in 1999. From September 2004 to August 2006, he was a Guest Researcher with the Signal and Systems Group, Uppsala University, Uppsala, Sweden. Since 2005, he has been a Full Professor with the School of Communications and Information Engineering, Xi'an University of Posts and Telecommunications, Xi'an. He has been the funded by over twenty projects including the National Natural Science Foundation of China, the 863 Program, and Important National Science and Technology Specific Projects. Due to his excellent contributions in education and research, he was awarded by the Program for New Century Excellent Talents in University, Ministry of Education, P. R. China, in 2009. His research interests include wireless communications, energy harvesting, cognitive radio and cooperative spectrum sensing. Currently, he is the President of Xi'an University of Posts and Telecommunications, and the Director of the Shaanxi Key Laboratory of Information Communication Network and Security.